THE ASTRONOMICAL JOURNAL, 2003 FEBRUARY, ASTRO-PH/YYMMNNN
Preprint typeset using LaTeX style emulateapj v. 19/02/01

X-RAY EMISSION FROM RADIO-QUIET QUASARS IN THE SDSS EARLY DATA RELEASE. THE $\alpha_{\rm ox}$ DEPENDENCE UPON UV LUMINOSITY

C. VIGNALI,[1] W. N. BRANDT,[1] AND D. P. SCHNEIDER[1]

Received 2002 September 14; accepted 2002 November 05

ABSTRACT

We investigate the X-ray properties of the color-selected radio-quiet quasars (RQQs) in the Sloan Digital Sky Survey (SDSS) Early Data Release using *ROSAT*, *Chandra* and XMM-*Newton* data. In the 0.16–6.28 redshift range, 136 RQQs have X-ray detections (69 from the *ROSAT* All-Sky Survey, RASS), while for 70 RQQs X-ray upper limits are obtained. The well-defined selection method utilized by the SDSS, coupled with the tight radio constraints from the FIRST/NVSS surveys, allow us to define a representative sample of optically selected RQQs whose broad-band spectral energy distributions (characterized by means of the optical-to-X-ray spectral index, $\alpha_{\rm ox}$) can be studied as a function of rest-frame ultraviolet (UV) luminosity and redshift. A partial correlation analysis applied to the SDSS sample (including the upper limits, but excluding the biased subsample of RASS detections) shows that $\alpha_{\rm ox}$ is a function of rest-frame UV luminosity (i.e., $\alpha_{\rm ox}$ steepens at high UV luminosities); this correlation is significant at the 3.7σ level. We do not detect a highly significant redshift dependence of $\alpha_{\rm ox}$. We also find a significant (7.8σ level) correlation between UV and X-ray luminosity. This correlation, parameterized by $L_{\rm X} \propto L_{\rm UV}^{0.75\pm0.06}$, extends previous results to the highest redshifts.

Subject headings: galaxies: active — galaxies: nuclei — quasars: general — X-rays: galaxies — surveys

1. INTRODUCTION

To date, many studies have focused on the dependence of quasar ultraviolet-to-X-ray spectral energy distributions [SEDs, often characterized by means of the spectral index $\alpha_{\rm ox}$=0.384 $\log(L_{2\ {\rm keV}}/L_{2500\ \rm Å})$] on luminosity and cosmic time. Quasars are known to exhibit strong luminosity evolution in the optical band (e.g., Boyle et al. 1994, 2000) and perhaps luminosity-dependent density evolution in the X-ray band (e.g., Miyaji, Hasinger, & Schmidt 2000; La Franca et al. 2002). A dependence of $\alpha_{\rm ox}$ on redshift would suggest different evolution in the optical and X-ray regimes.

Most previous studies agree that $\alpha_{\rm ox}$ is only marginally dependent upon redshift, the primary dependence of $\alpha_{\rm ox}$ being on 2500 Å luminosity (e.g., Avni & Tananbaum 1982, 1986; Marshall et al. 1984; Kriss & Canizares 1985; Tananbaum et al. 1986; Anderson & Margon 1987; Wilkes et al. 1994; Pickering, Impey, & Foltz 1994; Avni, Worrall, & Margon 1995). The only significant exception has been recently reported by Bechtold et al. (2002), who claimed that $\alpha_{\rm ox}$ depends primarily upon redshift. These studies were generally characterized by heterogeneous selection criteria or covered limited ranges of redshift or luminosity. Most investigations included both radio-quiet quasars (RQQs) and radio-loud quasars (RLQs). The X-ray properties of these two sub-classes of the quasar population are now well known to be different, with the RLQ emission often being dominated by the jets and enhanced by boosting (e.g., Wilkes & Elvis 1987; Worrall et al. 1987; Cappi et al. 1997). As discussed in §4.1.2.2 of Anderson (1985) and Appendix A of Anderson & Margon (1987), analyses of heterogeneous samples (such as RQQs and RLQs combined) with survival analysis techniques can lead to misleading results. Moreover, many previous samples also included Broad Absorption Line Quasars (BALQSOs). Recent studies (e.g., Gallagher et al. 2001, 2002; Green et al. 2001) have shown that, although BALQSOs are probably characterized by the same underlying X-ray continua as the majority of the quasar population, their X-ray emission is often depressed by large amounts of intrinsic absorption. This effect appears to apply to both low- and high-redshift BALQSOs (e.g., Brandt, Laor, & Wills 2000; Brandt et al. 2001; Vignali et al. 2001a; Gallagher et al. 2002). Although BALQSOs do not contribute greatly to the overall optically selected quasar population (≈ 10–15%; e.g., Weymann et al. 1991; §8.1 of Brandt et al. 2000; Tolea, Krolik, & Tsvetanov 2002), their inclusion can provide an "artificial" steepening of $\alpha_{\rm ox}$ as well as a larger, spurious scatter in any correlation study involving this spectral index (see Figure 4.1.2.2.a and the associated text in Anderson 1985).

Motivated by these considerations, we have started a project to investigate the dependence of $\alpha_{\rm ox}$ upon UV luminosity and redshift using the quasars discovered by the Sloan Digital Sky Survey (SDSS; York et al. 2000) and presently published mainly in the Early Data Release (EDR; Stoughton et al. 2002) quasar catalog[2] (Schneider et al. 2002). The SDSS provides a large and well-defined sample of optically selected quasars with a broad range in UV luminosity and redshift, suitable for such studies and to break degeneracies in the luminosity-redshift parameter space. We have focused on the RQQs, since they comprise the bulk of the quasar population (≈ 85–90%; e.g., Stern et al. 2000; Ivezic et al. 2002) and are not strongly affected by jet emission or boosting effects. For most of the objects, X-ray information has been obtained through analysis of *ROSAT* data. For the highest redshift (i.e., $z > 4$) quasars, however, we have also exploited the excellent capabilities of *Chandra* and XMM-*Newton*.

Throughout this paper we adopt H_0=70 km s^{-1} Mpc^{-1} in a Λ-cosmology with $\Omega_{\rm M}$=0.3 and Ω_Λ=0.7 (e.g., Lineweaver 2001). Note that most of the $\alpha_{\rm ox}$–log $L_{2500\ \rm Å}$ correlation papers previously cited used a H_0=50 km s^{-1} Mpc^{-1} and q_0=0.0

[1] Department of Astronomy & Astrophysics, The Pennsylvania State University, 525 Davey Laboratory, University Park, PA 16802 (chris@astro.psu.edu, niel@astro.psu.edu, and dps@astro.psu.edu).

[2] Available at http://archive.stsci.edu/sdss/quasars/edrqso.cat.

cosmology, which provides larger luminosities by factors of ≈ 2.0–6.5 in the redshift range ≈ 0–6.3.

2. THE SAMPLE: THE SDSS EARLY DATA RELEASE QUASAR CATALOG

The SDSS Early Data Release (EDR; Stoughton et al. 2002) contains 462 deg^2 of imaging data in five bands (designated u, g, r, i, and z; Fukugita et al. 1996; Gunn et al. 1998) and 54,008 spectra in the same area. The data were acquired in three regions: along the celestial equator in the southern Galactic sky, along the celestial equator in the northern Galactic sky, and in a region overlapping the SIRTF First Look Survey.[3] The SDSS EDR catalog of quasars consists of 3814 objects (3000 discovered by the SDSS) selected through a multicolor technique (similar to that described by Richards et al. 2002) down to magnitude limits of $i \approx 19$ and $i \approx 20$ for quasars below and above $z \approx 3$, respectively (Stoughton et al. 2002), with an overall expected completeness higher than 90%. In addition to the multicolor selection, a small percentage (≈ 0.5%) of SDSS targets were unresolved objects brighter than $i \approx 19$ that were coincident with FIRST radio sources (Becker, White, & Helfand 1995). The EDR quasars were selected in three stripes (each $\approx 2.5^\circ$ wide) over a slightly larger area (494 deg^2) than that covered by imaging observations, because some additional "interesting" fields were included (Stoughton et al. 2002). These quasars have at least one emission line with a full width at half maximum (FWHM) larger than 1000 km s^{-1}, luminosities higher than $M_{\rm i}$=-23 (for H_0=50 km s^{-1} Mpc^{-1}, q_0=0.5), and highly reliable redshifts ranging from 0.15 to 5.03. The EDR quasars used in this paper are those having the "quasar target flag" set to 1 in the EDR quasar catalog (column 22 in the quasar catalog; see §4 of Schneider et al. 2002). In this paper the SDSS EDR sample of quasars is extended to higher redshifts by including all of the published SDSS quasars up to $z = 6.28$ (e.g., Fan et al. 2001a) to place better constraints on the relevant correlations. The additional quasars represent only a small addition to the main EDR sample (≈ 2.6%); since they have been selected using a multicolor selection technique, we do not expect any significant bias to be introduced into the analysis.

2.1. *Selection of radio-quiet quasars*

The minority of EDR quasars selected based on their detection by FIRST (see §2) were immediately excluded from our study. Then from the color-selected SDSS quasars we have excluded all the RLQs, i.e., those quasars having a radio-loudness parameter,[4] R, larger than 10 (e.g., Kellermann et al. 1989). Radio flux densities at 1.4 GHz have been obtained either from FIRST or from NVSS (Condon et al. 1998), down to typical 3σ upper limits of 0.5 and 1.5 mJy, respectively. All of the quasars with X-ray coverage also have NVSS/FIRST coverage. Quasars characterized by loose radio-loudness upper limits (i.e., $R \lesssim 18$; only five in the sample of 206 SDSS quasars used in the following analysis) have been assumed to be radio quiet. Within the sample of SDSS quasars with X-ray coverage, the fraction of RQQs is ≈ 90%, which is in good agreement with previous estimates for optically selected quasars (e.g., Stern et al. 2000) and suggests that assuming the quasars with loose radio-loudness upper limits to be radio-quiet is reasonable.

2.2. *Optical magnitudes*

The magnitudes reported in the EDR catalog are generally accurate to 0.05 mag or better. To derive absolute luminosities for the SDSS quasars, the catalog magnitudes were first corrected for Galactic absorption using the *COBE*/DIRBE maps of Schlegel, Finkbeiner, & Davis (1998) and the scaling laws for the five SDSS filters reported in Schneider et al. (2002). The composite quasar spectrum presented in Vanden Berk et al. (2001), which was constructed using SDSS spectra of over 2000 quasars, was used to convert the broad-band *ugriz* measurements to flux densities at rest wavelengths of 2500 Å (required for $\alpha_{\rm ox}$ measurements) and 4400 Å (required to compute the radio-loudness parameter); this method accounts for emission lines as they pass through the SDSS filters. The offsets for both the rest-wavelength 2500 Å and 4400 Å flux densities as a function of redshift were calculated for each of the SDSS filters, using interpolation whenever possible. For example, if the observed wavelength of rest-frame 2500 Å occurred between the g and r filters, the value of the 2500 Å flux density was calculated using the relations for both the g and r filters, and the final measurement was the weighted average of the 2500 Å flux densities, weighted by the relative distances of $2500(1+z)$ Å from the central wavelengths of the g and r filters. If rest-wavelength 1280 Å occurred redward of the central wavelength of a filter, that filter was not used in the calculation, due to the large dispersion in the relations introduced by the presence of the Lyman α emission line and the Lyman α forest. If the observed-frame wavelength of the desired region of the spectrum was larger than the effective wavelength of the reddest filter, the relation for the reddest filter was used.

3. THE X-RAY DATA: DATA REDUCTION AND ANALYSIS

3.1. *The $z < 4$ sample: ROSAT observations*

The EDR quasar catalog was cross correlated with archival *ROSAT* data [pointed PSPC, pointed HRI, and the *ROSAT* All-Sky Survey (RASS)]. We used only the central regions (20′ radius) of the *ROSAT* PSPC and HRI detectors, where the sensitivity is highest and the PSPC window support structure does not affect source detection. This maximizes the probability of detecting faint sources. In cases of multiple observations of the same SDSS quasar, we chose the one with the best combination of off-axis angle and exposure time. Approximately 3.2% of the EDR area is covered by *ROSAT* pointed observations [considering only the inner 20′ of the *ROSAT* field-of-view; 37 PSPC fields (2 largely overlapping) and 11 HRI fields; see Fig. 1]. Source detection was performed in the 0.5–2 keV band for the PSPC and in the full band for the HRI, since no spectral information is available for the HRI. A conservative matching radius of 40″ was used to take into account the broadening of the Point Spread Function (PSF) at large off-axis angles.[5]

The pointed *ROSAT* PSPC and HRI data have been analyzed with the MIDAS/EXSAS package (Zimmermann et al. 1998). The sources have been detected by running the local detection algorithm LDETECT, the bicubic spline fit to the background map, and the map detection algorithm MDETECT.

[3] See http://sirtf.caltech.edu/SSC/fls.

[4] The radio loudness is parameterized by $R = f_{5\ \rm GHz}/f_{4400\ \rm Å}$ (rest frame). The rest-frame 5 GHz flux density is computed from the observed-frame 1.4 GHz flux density assuming a radio power-law slope of $\alpha = -0.8$, with $f_\nu \propto \nu^\alpha$.

[5] See ftp://ftp.xray.mpe.mpg.de/rosat/catalogues/1rxp/wga_rosatsrc.html.

The detection threshold of these algorithms was set at a likelihood of $L = -\ln(P_e) = 6$, corresponding to a probability P_e of the order of 2.5×10^{-3} that the observed number of photons in the source cell is produced entirely by a background fluctuation (corresponding to the $\approx 3\sigma$ detection level; Cruddace, Hasinger, & Schmitt 1988). In the present sample, the sources detected by the *ROSAT* PSPC (HRI) have typical offsets of less than 15–20″ (10″) from their optical positions, which are accurate to within 0.2″ (Schneider et al. 2002). This range of offsets is consistent with the values found recently by Vignali et al. (2001b) for faint hard X-ray selected sources in PSPC/HRI fields. All of the sources were inspected by eye to verify that they are not spurious fluctuations due to enhanced local background. Our previous experience (e.g., Vignali et al. 2001b) suggests that the combination of detection algorithms described above is quite effective at minimizing the number of spurious detections. We expect only ≈ 0.3 false sources in our sample due to background fluctuations adopting the detection threshold reported above. Assuming the integral 0.5–2 keV source counts of Hasinger et al. (1998), we conservatively expect $\lesssim 2$ spurious associations within the present sample of *ROSAT*-detected sources.

The background-subtracted, vignetting-corrected source counts were determined using the maximum likelihood method

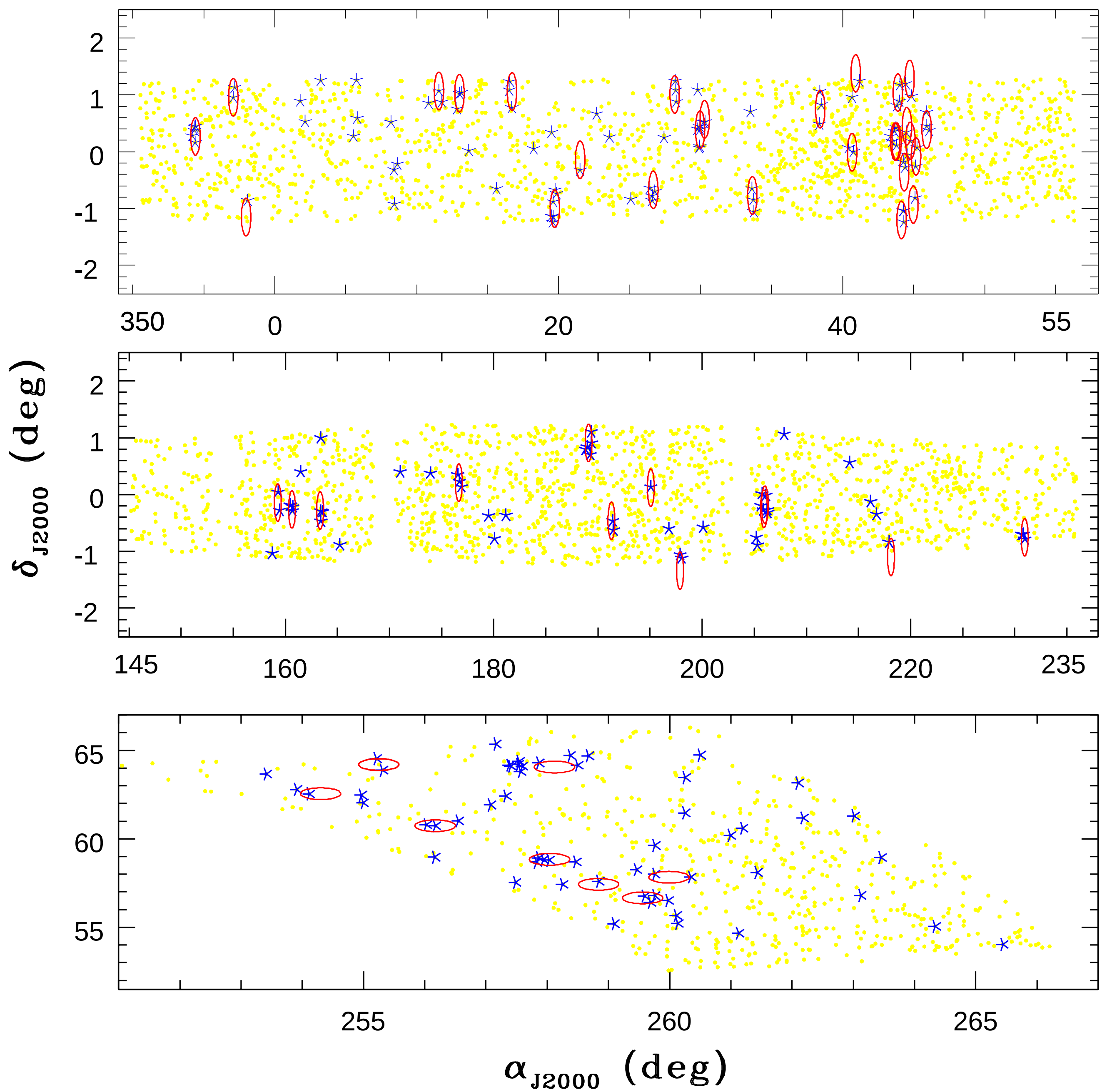

FIG. 1.— The *ROSAT* coverage of the SDSS EDR quasars (small points) with pointed PSPC and HRI observations (circles of radius 20′ in sky coordinates). The stars indicate the SDSS EDR RQQs used in this work. The small points in some circles are RLQs, which were not used in this work.

TABLE 1

NUMBERS OF SDSS RQQS IN *ROSAT*, *Chandra*, AND XMM-*Newton* OBSERVATIONS

Redshift Range	*ROSAT*					*Chandra*		XMM-*Newton*
	PSPC		HRI		RASS	ACIS		EPIC
	D	UL	D	UL	D	D	UL	D
$z < 2$	43	32	5	19	68	···	···	···
$2 < z < 4$	11	10	2	6	1	···	···	···
$z > 4$	···	···	···	···	···	5	3	1

NOTE. — "D" indicates the number of X-ray detections, while "UL" indicates the number of upper limits.

(MAXLIK). For the sources not detected in the *ROSAT* pointed observations, 3σ X-ray upper limits were computed using the SOSTA task in the XIMAGE package (Giommi et al. 1992) and an average value for the background close to the quasar position.

The same matching radius was utilized for the RASS data (see, e.g., Voges et al. 1999) in the 0.1–2.4 keV band with a slightly higher detection threshold [$L = -\ln(P_e) = 7$, the minimum available using the *ROSAT* Source Browser[6]]. The average exposure time for the quasars detected in the RASS is ≈ 1.2 ks.

3.1.1. *ROSAT results*

The results of the cross correlation of the SDSS EDR quasars with archival *ROSAT* data are presented in Table 1.

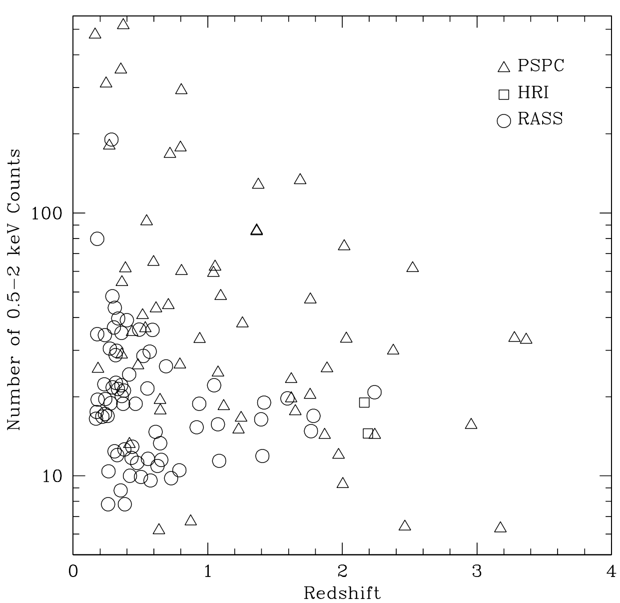

FIG. 2.— Number of counts (corrected for vignetting) in the 0.5–2 keV band for *ROSAT*–detected SDSS RQQs as a function of redshift. Triangles, squares, and circles represent pointed PSPC, pointed HRI, and RASS detections, respectively.

None of the SDSS EDR quasars at $z > 4$ lies in the inner 20′ of a *ROSAT* field. We found 54 X-ray detected RQQs in pointed PSPC fields, seven in pointed HRI fields, and 69 in the RASS. The numbers of upper limits were 42 and 25 for the PSPC and HRI, respectively. Only a small fraction ($\approx 4.7\%$) of the *ROSAT* pointed observations were targeting SDSS quasars (five detections and one upper limit); the relevant quasars are listed in Table 2 with a value of 0.0′ for the off-axis angle. The exclusion of the *ROSAT* targets from the following analyses does not change materially any of the results presented below. A plot of the number of counts from *ROSAT*-detected quasars as a function of redshift is shown in Fig. 2. Most of the X-ray detections are too faint to derive tight spectral constraints by means of hardness ratio analysis. Ten quasars have less than 10 counts in the 0.5–2 keV band (seven quasars at $z < 2$, two observed by the PSPC and five by the RASS; three at $2 < z < 4$, all observed by the PSPC). All of these faint objects satisfy the detection threshold because of the high sensitivity generally reached in the inner part of *ROSAT* field-of-view and the low background in some cases. These sources appear real after visual inspection, and in two out of five cases we were able to confirm the source's existence by analyzing an additional *ROSAT* PSPC observation (in the other cases no additional pointed observations were available).

Among the quasars with pointed *ROSAT* coverage, we found seven BALQSOs; one was detected by *ROSAT* and six were not. Unfortunately, no information about the presence of broad UV absorption features is available for $z \lesssim 1.5$ quasars due to the wavelength range of the SDSS spectrograph (3800–9200 Å; York et al. 2000). The relatively small fraction of BALQSOs within optically selected samples ($\approx$ 10–15%; e.g., Weymann et al. 1991; Brandt et al. 2000; Tolea et al. 2002) suggests that BALQSOs probably do not significantly contribute to the estimation of the average properties of the present sample at $z \lesssim 1.5$. We have searched in the NASA Extragalactic Database (NED) for published UV spectra of the SDSS quasars at $z \lesssim 1.5$. A small fraction (below 1%) of the low-redshift SDSS quasars have UV coverage, and none of these shows broad absorption features. In §4.3 and §4.4 we will statistically estimate the impact of BALQSOs on α_{ox} determinations at $z \lesssim 1.5$.

3.2. *The $z > 4$ sample: Chandra and XMM-Newton observations*

All but one of the $z > 4$ SDSS quasars in the X-ray sample have been observed by *Chandra*, the only exception being the $z = 5.74$ quasar (Fan et al. 2000b) detected by XMM-*Newton* (Brandt et al. 2001). This quasar has recently been revealed to be a BALQSO (Maiolino et al. 2001; Goodrich et al. 2001). The *Chandra* results reported in this paper have been taken from Vignali et al. (2001a; five SDSS RQQs, two of which are X-ray undetected BALQSOs) and Brandt et al. (2002; two SDSS RQQs). *Chandra* data for one additional SDSS RQQ have been retrieved from the archive (also published by Bechtold et al. 2002). All of the *Chandra* sources were ob-

[6] Available at http://www.xray.mpe.mpg.de:80/cgi-bin/rosat/src-browser.

served with the back-illuminated ACIS-S/S3 CCD (Garmire et al. 2002). Source detection was carried out with WAVDETECT (Freeman et al. 2002). For each image, we calculated wavelet transforms (using a Mexican hat kernel) with wavelet scale sizes of 1, 1.4, and 2 pixels using a false-positive probability threshold of 10^{-6} (see Vignali et al. 2001a for further information about the *Chandra* reduction and detection processes).

To increase the number of quasars at $z > 4$ populating the high-luminosity tail of the luminosity function, and therefore to place stronger constraints on the parameters involved in this study, we will also include in the analysis 13 luminous RQQs taken from the Palomar Digital Sky Survey (DPOSS; Djorgovski et al. 1998; hereafter referred to as PSS) which have been observed by *Chandra* (Vignali et al. 2001a, 2003). Twelve of these objects are detected in the soft (0.5–2 keV) X-ray band. Given their high luminosities, these objects are sufficiently bright that any quasars of this class that fall in the SDSS survey area will be included in the SDSS spectroscopic survey (indeed, many PSS quasars have already been recovered by the SDSS; see Schneider et al. 2002 and references therein). Therefore, we do not expect to introduce biases by including PSS quasars in our otherwise pure SDSS sample. The critical results below will be given both with and without inclusion of the PSS quasars.

3.2.1. *Chandra and XMM-Newton results*

A summary of the *Chandra* and XMM-*Newton* results for $z > 4$ SDSS RQQs is presented in Table 1. We found six X-ray detected SDSS RQQs and three upper limits, two of which are associated with BALQSOs (see Vignali et al. 2001a for a detailed discussion). The last X-ray undetected quasar is peculiar; its optical spectrum is characterized by a lack of emission lines (Fan et al. 1999, 2000a).

3.3. *Count rate-to-flux conversion*

All of the X-ray fluxes reported in this paper have been converted into the observed 0.5–2 keV band and corrected for Galactic absorption. The count rate-to-flux conversion was computed using the Portable, Interactive, Multi-Mission Simulator (PIMMS Version 3.2c; Mukai 2001) software for a power-law photon index[7] of $\Gamma = 2$ and Galactic absorption (Dickey & Lockman 1990). Samples of $z \approx 0$–2 RQQs are well fitted in the 2–10 keV band by power-law continua with Γ=1.7–2.3 (e.g., George et al. 2000; Mineo et al. 2000; Reeves & Turner 2000). Although there have been claims of a possible flattening of X-ray spectral continua at $z \approx 2$ (e.g., Vignali et al. 1999; Blair et al. 2000), the assumption of a flatter slope ($\Gamma = 1.5$) has only a few percent effect ($\approx$ 1–2%) on the derived fluxes. In the same manner, assuming a steeper power-law slope ($\Gamma = 2.5$) has a few percent effect on the derived fluxes. It must also be kept in mind that, given the large redshift range of the SDSS quasars used here, we are not sampling the same rest-frame X-ray bandpass for the entire SDSS sample; therefore the assumption of a single power-law model for the count rate-to-flux conversion may be too simplistic. However, although the direct spectral information available for $z > 2$ high-luminosity RQQs is still limited, there are indications that quasars at the highest redshifts are also well parameterized by $\Gamma \approx 2$ power-law X-ray continua (e.g., Dewangan et al. 2002; Page et al. 2002; Vignali et al. 2003).

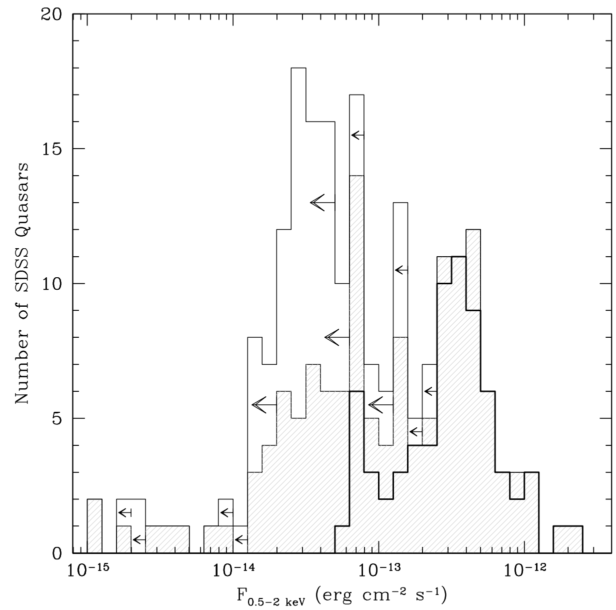

FIG. 3.— Galactic absorption-corrected 0.5–2 keV flux distribution for the 206 SDSS RQQs with X-ray information. The shaded area indicates the quasars with X-ray detections, the thin continuous line those from the entire sample, and the thick line the ones detected by the RASS. Unshaded areas with arrows indicate upper limits.

The observed-frame 0.5–2 keV flux distribution for our sample is plotted in Fig. 3. Most of the X-ray brightest objects have been detected by the RASS (thick continuous line).

3.4. *SDSS RQQs observed in the X-ray band*

The combined SDSS, *ROSAT*, *Chandra*, and XMM-*Newton* data allow a systematic study of the ultraviolet-to-X-ray properties of SDSS RQQs in the redshift range z=0.16–6.28. A total of 206 RQQs have X-ray information: 136 have been detected, while for 70 RQQs 3σ upper limits have been derived. Systematic cross-calibration errors might be present when data from different X-ray instruments are analyzed. However, to date we have no indication of any *ROSAT* versus *Chandra* cross-calibration problems (T. Gokas 2002, private communication).[8] The principal optical, X-ray, and radio information for the SDSS RQQs with X-ray coverage is summarized in Table 2.[9] In Fig. 4 we compare the redshift and rest-frame 2500 Å luminosity density distributions of the X-ray detected SDSS quasars (shaded area) with the overall sample of SDSS quasars with X-ray information (thin continuous line). The thick line shows the SDSS RQQs detected by the RASS, most of which are at $z < 1.5$. The sample has a fairly high fraction of X-ray detections ($\approx$ 49% if only pointed observations are taken into account). Among the 206 SDSS RQQs, 11 objects at low redshift are optically resolved (Schneider et al. 2002). They do not populate a particular region in the optical–X-ray luminosity space, suggesting that the emission from their host galaxies is likely to be negligible.

[7] Γ=$-\alpha$+1; $N(E) \propto E^{-\Gamma}$, where $N(E)$ has units of photons cm^{-2} keV^{-1} s^{-1}.

[8] See also http://cxc.harvard.edu/cal/Links/Acis/acis/Presentations/cross_cal/wa2-snowden.

[9] This table is also available at http://www.astro.psu.edu/users/niel/papers/papers.html.

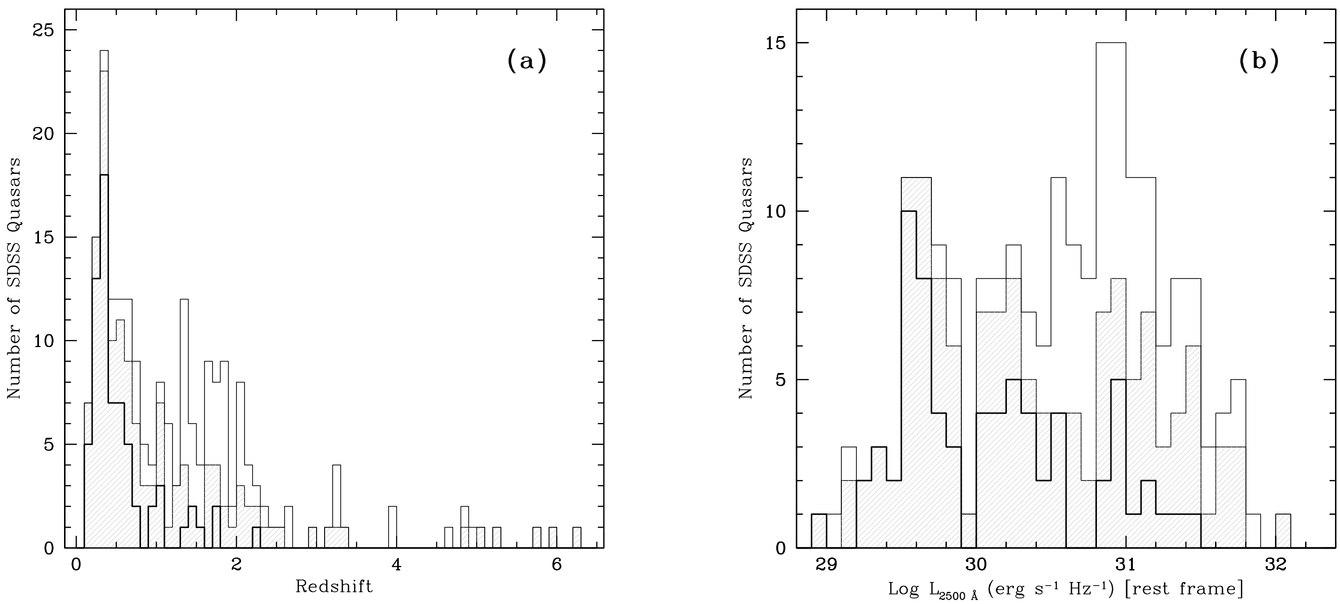

FIG. 4.— (a) Redshift and (b) rest-frame 2500 Å luminosity density distributions for the 206 SDSS RQQs in *ROSAT*, *Chandra*, and XMM-*Newton* observations. The shaded area indicates X-ray detections, the thin continuous line indicates the whole sample, and the thick line shows the RQQs detected by the RASS.

4. BROAD-BAND PROPERTIES OF SDSS QUASARS

One of the main goals of this paper is to study the broad-band properties of SDSS RQQs, parameterized by the optical-to-X-ray spectral index $\alpha_{\rm ox}=\frac{\log(f_{2\,\rm keV}/f_{2500\,Å})}{\log(\nu_{2\,\rm keV}/\nu_{2500\,Å})}$, as a function of rest-frame UV luminosity density and redshift. Working with non-simultaneous UV and X-ray data will have some effects on the derived individual $\alpha_{\rm ox}$ values, but since our samples are fairly large we do not expect significant biases when the samples are considered as a whole. As most of the papers cited in §1 have focused on the relationship between rest-frame 2500 Å luminosity density (hereafter referred to as l_{uv}=log $L_{2500\,Å}$) and rest-frame 2 keV luminosity density (hereafter referred to as l_x=log $L_{2\,\rm keV}$), we will address this issue as well. The choice of using luminosity densities instead of flux densities is based on several arguments, as stated in Kembhavi, Feigelson, & Singh (1986), and generally provides more robust results. However, this choice introduces a possible bias into the analysis, as luminosity is strongly correlated with redshift in flux-limited samples. It is therefore crucial to estimate the influence of this effect on the correlations in order to draw reliable conclusions about true physical relationships. In this paper, this has been achieved with the partial correlation analysis technique developed for use with censored data (Akritas & Siebert 1996).

4.1. *The technique: Partial correlation and regression analysis*

A partial correlation analysis investigates the correlation of two variables while controlling for (holding constant) a third or additional variables. Partial correlation analysis requires meeting all of the assumptions of Pearsonian correlation, e.g., the linearity of the relationships (including that between the original variables and the control variable). The method used in this paper is that described by Akritas & Siebert (1996); this allows one to apply partial correlation to censored data and to assign a significance level to the resulting correlation coefficient based on the Kendall τ-statistic (Kendall 1970). When a significant (at the $\gtrsim 3\sigma$ confidence level) correlation is found according to the partial correlation analysis, its basic parameters are quantified via regression analysis, taking into account upper limits. For this purpose, we have used the ASURV software package Rev 1.2 (LaValley, Isobe, & Feigelson 1992), which implements the survival analysis methods presented in Feigelson & Nelson (1985) and Isobe, Feigelson, & Nelson (1986). We used the EM (Estimate and Maximize) regression algorithm (Dempster, Laird, & Rubin 1977) and the Buckley-James (Buckley & James 1979) regression method.

4.2. *The ROSAT sample used in the $\alpha_{\rm ox}$ study*

Among the SDSS RQQs with *ROSAT* coverage, in the $\alpha_{\rm ox}$ study we have used only the 128 RQQs covered by pointed PSPC and HRI observations. As shown in Fig. 3, the quasars detected by the RASS are strongly concentrated at bright X-ray fluxes, with most of the sources being brighter than 10^{-13} erg cm^{-2} s^{-1} in the observed-frame 0.5–2 keV band. Although the RASS covers 99.8% of the sky, typical exposure times are $\approx$ 300–400 s for most of the fields, which are not suitable for providing useful constraints on $\alpha_{\rm ox}$ for our sample. Including both the pointed and RASS data (detections and upper limits) in the $\alpha_{\rm ox}$ survival analyses below would likely lead to spurious results, as our sample would be dominated by weak RASS upper limits and would thus suffer from severe pattern censoring problems (see §4.1.2.1 of Anderson 1985 and Appendix A of Anderson & Margon 1987).

The $\alpha_{\rm ox}$ distribution of SDSS RQQs (excluding the RASS detections) is shown in Fig. 5 (the shaded area indicates the $\alpha_{\rm ox}$ values for X-ray detected quasars). Taking into account upper limits using ASURV, the average $\alpha_{\rm ox}$ is -1.65 ± 0.02. Note, however, that a dependence of $\alpha_{\rm ox}$ upon luminosity is likely present (see §4.4).

One object in our sample, SDSSp J030422.39+002231.7 at z = 0.638, is characterized by a notably steep $\alpha_{\rm ox}$ (-2.01), which suggests it could be a BALQSO or mini-BALQSO (e.g., Brandt et al. 2000). Its optical spectrum is quite blue and shows no obvious absorption near Mg II. However, the [O III] 5007Å line is quite weak and the Fe II emission-line blends are strong (G. Richards 2002, private communication). These properties have been seen from many low-ionization BALQSOs and other soft X-ray weak quasars (e.g., Boroson & Meyers 1992; Turnshek et al. 1997; Laor & Brandt 2002).

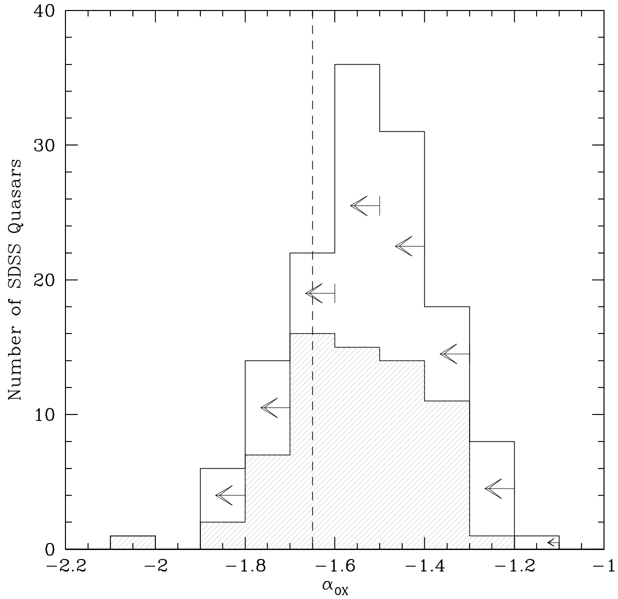

FIG. 5.— Histogram of the α_{ox} distribution for SDSS RQQs with coverage in pointed X-ray observations. The shaded area indicates the quasars with X-ray detections, while the continuous line indicates those from the entire sample. Unshaded areas with arrows indicate α_{ox} upper limits. The vertical dashed line at α_{ox}=−1.65 indicates the average α_{ox} calculated in §4.2.

4.3. *The effect of unknown BALQSOs at $z \lesssim 1.5$ on* α_{ox} *measurements*

As mentioned in §3.1.1, at $z \lesssim 1.5$ it is not possible to identify BALQSOs among the quasars from SDSS spectra. However, their importance in average α_{ox} determinations can be estimated statistically. Given the high fraction of X-ray undetected BALQSOs at $z > 1.5$ (80%) and the general evidence that BALQSOs have strongly depressed X-ray emission in the 0.5–2 keV band (see §1), we have randomly removed from the $z < 1.5$ subsample (69 RQQs with 39 X-ray detections) a variable number (10–15% of this subsample) of X-ray non-detections. Taking into account the upper limits using ASURV, the average α_{ox} at $z < 1.5$ is $\langle\alpha_{ox}\rangle = -1.61 \pm 0.03$. By randomly excluding some of the X-ray non-detections as previously described, we obtain $\langle\alpha_{ox}\rangle = -1.58 \pm 0.03$, close to the previous value. It must be kept in mind that some BALQSOs could be detected at $z < 1.5$; therefore the previous average value of −1.58 would represent a conservative estimate.

4.4. α_{ox} *versus redshift and 2500 Å luminosity density*

The α_{ox} distributions as a function of redshift (Fig. 6a) and 2500 Å luminosity density (Fig. 7a) are characterized by large scatter, which prevents one from easily identifying a trend. To shed light on this issue, we averaged the α_{ox} values in redshift (Fig. 6b) and luminosity (Fig. 7b) bins taking into account the upper limits. The flat α_{ox} value found in the redshift range $3 < z < 4$ is likely to be due to the small number of objects (eight RQQs, five of which are non-detections). A trend of decreasing α_{ox} as a function of redshift and luminosity can be seen in both distributions, although it is not possible to determine which anti-correlation is the most important one or to quantify the significance without applying partial correlation analysis. It must be kept in mind that a certain degree of anti-correlation is expected between α_{ox} and log $L_{2500\,\text{Å}}$, given the presence of the UV luminosity

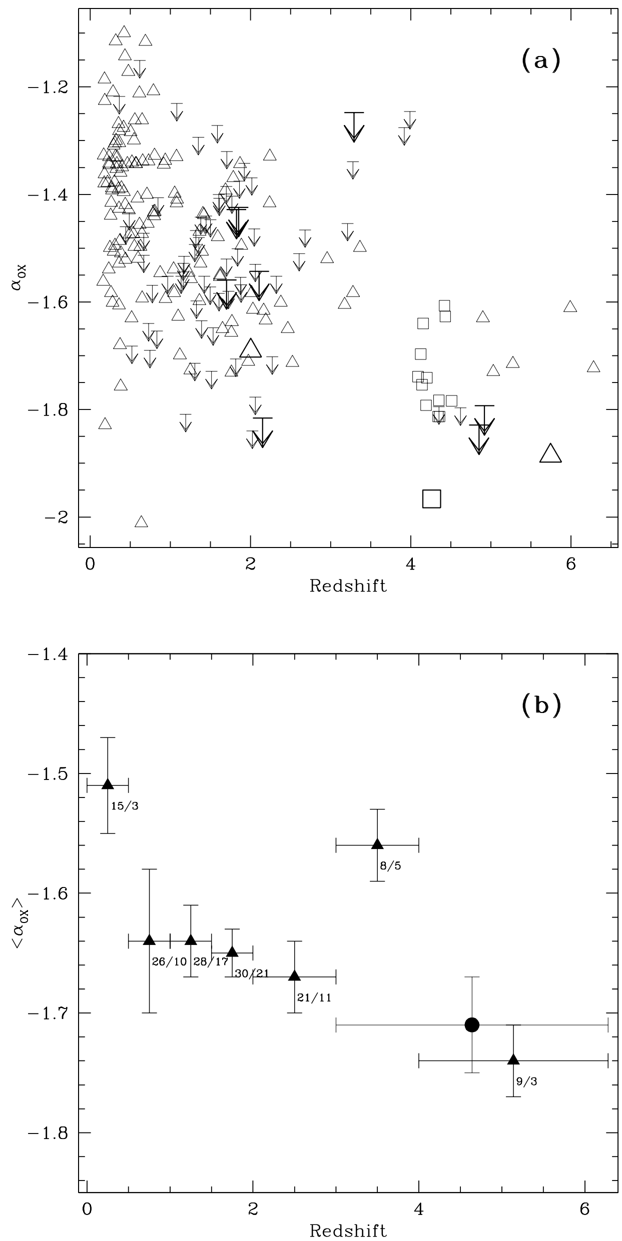

FIG. 6.— (a) α_{ox} distribution of RQQs as a function of redshift. SDSS RQQs are shown as triangles (X-ray detections) and downward-pointing arrows (X-ray upper limits). The open squares indicate the PSS quasars (12 X-ray detected RQQs and one upper limit). Larger and thicker symbols indicate the BALQSOs. (b) Average α_{ox} indices as a function of redshift for the SDSS RQQs only. The α_{ox} values have been averaged using ASURV (LaValley et al. 1992). The two numbers associated with each data point (triangles) indicate the total number of quasars and the number of upper limits in each redshift interval (whose range is shown by the x-axis bar), respectively. The y-axis error bars represent the standard deviation of the mean (as determined with ASURV). To improve the statistics, the average α_{ox} value obtained using all quasars at $z > 3$ is also displayed (filled circle).

term in the α_{ox} formula (see §4.5 for further discussion).

The measured values of α_{ox} show no strong dependence upon redshift (2.1σ; 1.7σ when the BALQSOs are removed from the analysis; see Table 3) from the partial correlation analysis. We also searched for possible α_{ox}–redshift dependencies in individual redshift/luminosity bins, but found none. The inclusion of the 13 PSS quasars (see §3.2; open squares in Fig. 6a) provides a slightly, but not sufficiently, better significance of the above anti-correlation (2.8σ; 2.3σ when the BALQSOs are removed).

TABLE 3
CORRELATIONS AND THEIR SIGNIFICANCES FROM PARTIAL CORRELATION ANALYSIS

	α_{ox}–z	α_{ox}–l_{uv}
SDSS only, with BALQSOs	2.1σ	3.7σ
SDSS only, without BALQSOs	1.7σ	3.4σ
SDSS and PSS, with BALQSOs	2.8σ	3.8σ
SDSS and PSS, without BALQSOs	2.3σ	3.9σ

Applying the partial correlation analysis, we find that the α_{ox}–l_{uv} anti-correlation (hereafter parameterized by the equation $\alpha_{ox} = A_1\, l_{uv} + B_1$) is significant at the 3.7σ level (3.4σ level) when the BALQSOs are included (excluded) in the analysis (see Table 3). According to the EM regression, the parameters of this relationship are

$$A_1 = -0.11 \pm 0.02 \quad B_1 = 1.85 \pm 0.69 \ \text{(including BALQSOs)} \tag{1}$$

$$A_1 = -0.10 \pm 0.02 \quad B_1 = 1.32 \pm 0.70 \ \text{(excluding BALQSOs)}. \tag{2}$$

The first parameterization is shown in Fig. 7a as a dashed line. Similar values are found using the Buckley-James regression method. Using the same approach described in §4.3, we evaluated the impact of possible unknown BALQSOs in the partial correlation analysis by randomly removing ≈ 10% of the X-ray non-detections at $z < 1.5$. The α_{ox}–l_{uv} anti-correlation is slightly more significant after this procedure. The α_{ox}–l_{uv} anti-correlation becomes slightly more significant (3.8σ) after the inclusion of the PSS quasars in the analysis (open squares in Fig. 7a), with similar best-fit parameters. Our finding above that α_{ox} depends primarily on l_{uv} is consistent with the fact that the α_{ox} dependence upon l_{uv} in Fig. 7b appears somewhat stronger than the α_{ox} dependence upon redshift in Fig. 6b. Given the dependence of α_{ox} upon l_{uv}, the assumption of the same α_{ox} value regardless of the UV luminosity density of a quasar can imply up to a factor of ≈ 3 error in estimating its soft X-ray flux.

It is worth noting that ≈ 5–10% of $z \approx 4$–6 quasars may experience a factor $\gtrsim 2$ magnification due to gravitational lensing (e.g., Wyithe & Loeb 2002; Comerford, Haiman, & Schaye 2002), assuming the SDSS luminosity function reported by Fan et al. (2001b) for $M_B < -26$ SDSS quasars [$\phi(L) \propto L^{\beta}$, with $\beta \approx -2.5$]. For steeper luminosity functions, the fraction of high-redshift lensed quasars may increase to ≈ 30% (e.g., Wyithe & Loeb 2002). Such an effect will confuse studies of the dependence of α_{ox} (which should not be changed by lensing, unless the UV and X-ray luminosities are magnified differently) upon luminosity. Imaging of known $z > 4$ quasars with *HST* will soon constrain the fraction of gravitationally lensed high-redshift quasars (M. Strauss 2002, private communication). We have roughly estimated the importance of such an effect by randomly reducing by a factor ≈ 2–5 the UV luminosity densities of ≈ 10% (i.e., 2–3 objects) of the $z > 4$ quasars, including the PSS sample. The partial correlation results from this exercise do not change significantly from the previous analysis; the α_{ox}–l_{uv} relation is still present.

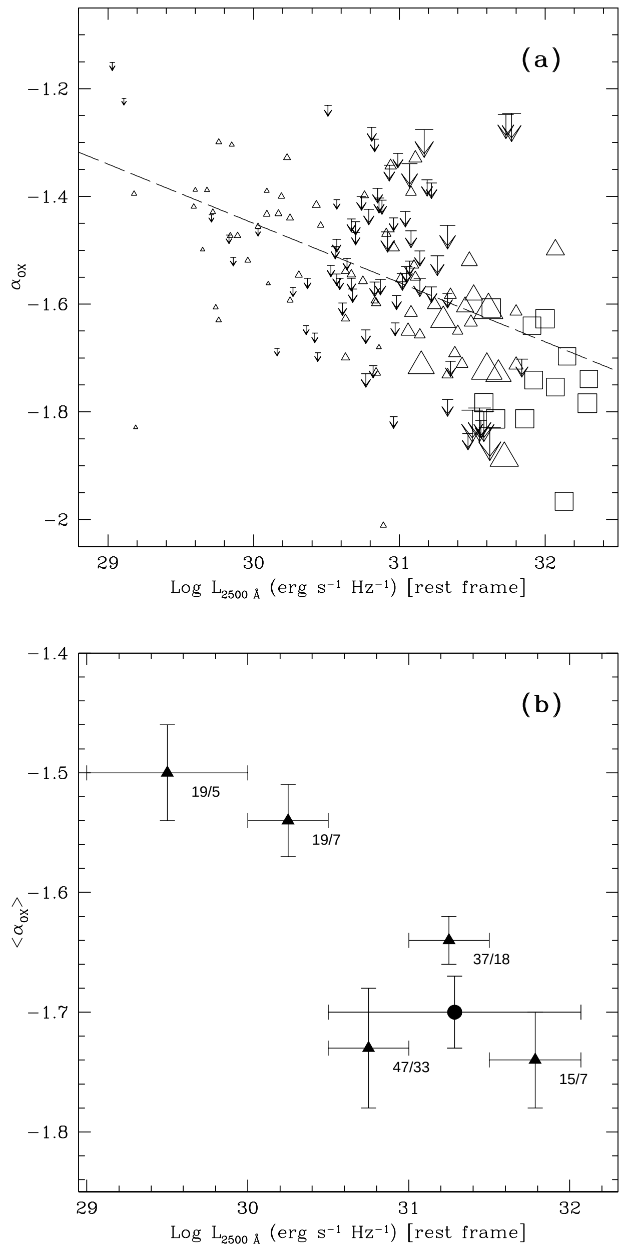

FIG. 7.— (a) α_{ox} distribution as a function of rest-frame 2500 Å luminosity. The sizes of the symbols (triangles for the SDSS X-ray detected RQQs and downward-pointing arrows for the upper limits) increase as a function of redshift. The open squares indicate the PSS quasars (12 X-ray detected RQQs and one upper limit). The dashed line indicates the relationship obtained with the pure SDSS sample using ASURV and including the BALQSOs (equation 1). (b) Average α_{ox} indices as a function of rest-frame 2500 Å luminosity for the SDSS RQQs only. The α_{ox} values have been averaged using ASURV (LaValley et al. 1992). The two numbers associated with each data point indicate the total number of quasars and the number of upper limits in each luminosity interval (whose range is shown by the x-axis bar), respectively. The y-axis error bars represent the standard deviation of the mean. To improve the statistics, the average α_{ox} value obtained using all quasars at l_{uv}>30.5 erg s^{-1} Hz^{-1} is also displayed (filled circle).

Finally, we have assessed if our main results above are sensitive to our chosen cosmology by repeating our analyses with a H_0=50 km s^{-1} Mpc^{-1} and q_0=0.0 cosmology (see §1). Our main results appear qualitatively unchanged for this choice of cosmology.

4.5. *l_x versus l_{uv}*

Previous studies of optically selected quasars have found a strong correlation between optical and X-ray luminosity densities (e.g., Zamorani et al. 1981), parameterized by $l_x \propto l_{uv}{}^{\beta}$, with β typically varying from ≈ 0.7 (e.g., Pickering et al. 1994; Wilkes et al. 1994) to ≈ 0.8 (e.g., Avni & Tananbaum 1986). Most of these studies were based on *Einstein* data, and the results were obtained using the Detection and Bounds method described by Avni et al. (1980), i.e., taking into account both detections and upper limits. Using a different approach, stacking analysis, Green et al. (1995) obtained a similar result ($\beta \approx 0.86$) for a sample of Large Bright Quasar Survey (LBQS; Hewett, Foltz, & Chaffee 1995) quasars observed in the RASS. On the other hand, a study by La Franca et al. (1995), based on *Einstein* data, found that the slope for the ultraviolet–X-ray relationship was consistent with unity using the modified orthogonal distance regression method (Fasano & Vio 1988), which accounts for errors in both variables and intrinsic scatter in the data. However, as pointed out by Yuan et al. (1998a), the significant dispersion in the data and, possibly, their inhomogeneous object selection, could induce a steeper correlation slope.

Finding a non-linear l_x–l_{uv} correlation (with a slope less than unity) for our SDSS sample of RQQs would support our previous results (see §4.4) in a totally unbiased way. While a certain degree of anti-correlation is expected between $\alpha_{\rm ox}$ and l_{uv} given the presence of the UV luminosity term in the $\alpha_{\rm ox}$ formula, no correlation is mathematically expected *a priori* between l_x and l_{uv}. With the present work we confirm previous results about the existence of a strong correlation between l_x and l_{uv}, with an extension to the highest redshifts/luminosities given the inclusion of $z > 4$ quasars recently observed by *Chandra* and XMM-*Newton*. We used the generalized Kendall τ-statistic (Brown, Hollander, & Korwar 1974) to evaluate the significance of the result, and the EM algorithm (Dempster et al. 1977) and the Buckley-James method (Buckley & James 1979) to derive the parameters of the relationship. We find a significant correlation (see Fig. 8), parameterized by

$$l_x \propto l_{uv}{}^{0.71\pm0.06} \quad \text{(including BALQSOs; 7.8}\sigma\text{ significance level)} \tag{3}$$

and

$$l_x \propto l_{uv}{}^{0.75\pm0.06} \quad \text{(excluding BALQSOs; 7.9}\sigma\text{ significance level)} \tag{4}$$

The latter correlation is shown in Fig. 8 (dashed line). For comparison purposes, the dotted line shows a correlation with $\beta = 1$ constrained to pass through the mean l_x and l_{uv}.

The inclusion of the PSS quasars at $z > 4$ has the effect of increasing the significance of this correlation up to 9.3σ (both with and without the BALQSOs), and the basic parameters of the correlation remain unchanged. The significance of this correlation over a large redshift and luminosity range suggests that it is a universal property of optically selected (and also X-ray selected; e.g., La Franca et al. 1995) quasars.

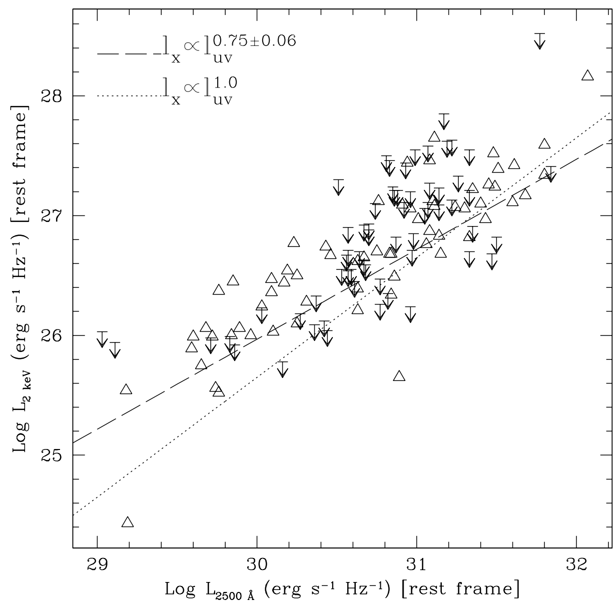

FIG. 8.— l_x versus l_{uv}. Triangles indicate SDSS RQQs observed in pointed X-ray observations (excluding BALQSOs). The dashed line indicates the best-fit relationship obtained when BALQSOs are excluded from the analysis. For comparison purposes, the dotted line shows a correlation with $\beta = 1$, constrained to pass through the average l_x and l_{uv}.

We have investigated if β has any redshift dependence. Using the RQQs at $z < 1.5$ ($z > 1.5$) we find $\beta = 0.61 \pm 0.11$ ($\beta = 0.90 \pm 0.19$ excluding BALQSOs and $\beta = 0.79 \pm 0.20$ including BALQSOs); the division at $z = 1.5$ has been chosen to give approximately the same number of objects in each redshift interval. Therefore, we do not detect any highly significant variation of β with redshift.

Using the definition of $\alpha_{\rm ox}$, the equation $\alpha_{\rm ox} = A_1\, l_{uv} + B_1$ (see §4.4), and $l_x \propto l_{uv}{}^{\beta}$, we can derive A_1 as a function of β and some constant terms. Using the range of l_{uv} for our SDSS sample and the constant terms reported in equations (2) and (4), we derive $A_1 \approx -0.10$. This is entirely consistent with the value reported in equation (2).

5. DISCUSSION

5.1. *Results from the SDSS RQQ sample*

We have presented the X-ray properties of the color-selected SDSS RQQs, mainly taken from the EDR, using *ROSAT*, *Chandra*, and XMM-*Newton* data. In the 0.16–6.28 redshift range, we detect 67/137 SDSS RQQs covered by pointed X-ray observations and an additional 69 SDSS RQQs observed by the RASS. We have used the unbiased sample of 137 RQQs with pointed X-ray observations to investigate the dependence of the $\alpha_{\rm ox}$ index upon rest-frame 2500 Å luminosity and redshift using partial correlation analysis applied to censored X-ray data. The principal results of our study are the following:

- The optical-to-X-ray spectral slope, $\alpha_{\rm ox}$, is anti-correlated with l_{uv} at the 3.4–3.7σ significance level, although the scatter in this anti-correlation is large (see §4.4). The inclusion of 13 $z > 4$, high-luminosity PSS quasars increases slightly the significance of the $\alpha_{\rm ox}$–l_{uv} anti-correlation to 3.8–3.9σ. There is no significant correlation between $\alpha_{\rm ox}$ and redshift, even when the sample of PSS quasars is included. These results suggest that the mechanism driving quasar broad-band emission (i.e., accretion onto a super-massive black hole) is similar in the local and the early Universe. They also indicate that, although it is likely that high-redshift quasars are radiating at higher fractions of their Eddington luminosity (e.g., Kauffmann & Haehnelt 2000), no unusual phenomena such as accretion-disk instabilities (e.g., Lightman & Eardley 1974; Shakura & Sunyaev 1976) or "trapping radius" effects (e.g., Begelman 1978; Rees 1978) seem to be dominant. It appears that already at $z \approx 6$ quasars are almost completely built-up systems, even though the time available was short at those epochs ($\lesssim 1$ Gyr in our cosmology).

- We confirm the l_x–l_{uv} correlation as being an intrinsic property for optically selected RQQs. This correlation can be parameterized by $l_x \propto l_{uv}^{0.75\pm0.06}$, in good agreement with most previous work.

5.2. *Comparison with earlier work*

The $\alpha_{\rm ox}$ dependence upon luminosity and redshift has been studied for many years. However, most earlier studies, although generally providing results consistent with ours (i.e., $\alpha_{\rm ox}$ depends mainly upon l_{uv}), were limited by heterogeneous selection criteria of the samples (e.g., Avni et al. 1995) or limited coverage in redshift/luminosity. As pointed out by Yuan, Siebert, & Brinkmann (1998b) using Monte-Carlo simulations, a spurious anti-correlation between $\alpha_{\rm ox}$ and UV luminosity density can emerge even for a population with an intrinsically constant $\alpha_{\rm ox}$, provided that the dispersion of the UV luminosities is similar to or larger than that of the X-ray luminosities. Analysis of the dispersions of l_{uv} and l_x for the SDSS RQQs used in this work indicates that the $\alpha_{\rm ox}$–l_{uv} anti-correlation is likely to be real.

The lack of sensitive radio surveys (e.g., FIRST, Becker et al. 1995; NVSS, Condon et al. 1998) prevented the early studies of quasars from clearly discriminating between the radio-quiet and radio-loud populations (except for the sources detected at high radio flux densities); these two populations have been known to have different emission properties in the X-ray band since *Einstein* (e.g., Zamorani et al. 1981; Wilkes & Elvis 1987). In this regard, the sensitive radio coverage for all of the quasars used in our study allowed us to select a sample of "pure" RQQs without contamination by radio-loud objects.

The only results indicating that $\alpha_{\rm ox}$ depends upon redshift have been presented by Yuan et al. (1998a) and Bechtold et al. (2002). Yuan et al. (1998a), using a large database of RQQs seen in the RASS and *ROSAT* pointed observations, found that $\alpha_{\rm ox}$ depends on 2500 Å luminosity at $l_{uv} > 30.5$ erg s^{-1} Hz^{-1} and slightly on redshift at $z < 0.5$. We did not find the latter dependence, but the number of SDSS RQQs with X-ray coverage at $z < 0.5$ is small (15 RQQs). Bechtold et al. (2002) reported a significant $\alpha_{\rm ox}$–redshift anti-correlation for a large sample of quasars observed by *ROSAT* (data taken from Yuan et al. 1998a) and *Chandra* over the same redshift range as our study. The heterogeneous selection and construction criteria of the Bechtold et al. (2002) sample, coupled with the lack of a partial correlation analysis, might lead to different results than ours.

5.3. *Future possibilities and work*

Studies using a larger number of objects and, hopefully, a higher fraction of X-ray detections are required to address all the issues related to $\alpha_{\rm ox}$ dependences upon luminosity or redshift. A larger number of SDSS quasars will soon become available to the scientific community with the next data release, which will provide a factor of ≈ 5 increase in the number of SDSS optically selected objects. From an X-ray perspective, most of these quasars are likely to be detected easily with snapshot observations by modern X-ray satellites. Furthermore, given the large field-of-view of the EPIC instruments onboard XMM-*Newton* ($\approx 15'$ radius), we expect a sizeable number of serendipitously observed SDSS RQQs in the next few years.

We gratefully acknowledge the financial support of *Chandra* X-ray Center grant DD1-2012X (CV, WNB, DPS), NASA LTSA grant NAG5-8107 (CV, WNB), and NSF grant AST99-00703 (DPS). We thank M. G. Akritas, D. M. Alexander, S. F. Anderson, F. E. Bauer, A. Comastri, E. D. Feigelson, L. Pozzetti, G. Richards, and G. Zamorani for interesting and thoughful discussions, and J. Englhauser for help with the RASS archive. CV also acknowledges partial support from the Italian Space Agency, under the contract ASI I/R/113/01, and from the Ministry for University and Research (MURST) under grant Cofin-00-02-36.

Funding for the creation and distribution of the SDSS Archive has been provided by the Alfred P. Sloan Foundation, the Participating Institutions, the National Aeronautics and Space Administration, the National Science Foundation, the U.S. Department of Energy, the Japanese Monbukagakusho, and the Max Planck Society. The SDSS Web site is http://www.sdss.org/. The SDSS is managed by the Astrophysical Research Consortium (ARC) for the Participating Institutions. The Participating Institutions are the University of Chicago, Fermilab, the Institute for Advanced Study, the Japan Participation Group, the Johns Hopkins University, Los Alamos National Laboratory, the Max-Planck-Institute for Astronomy (MPIA), the Max-Planck-Institute for Astrophysics (MPA), New Mexico State University, the University of Pittsburgh, Princeton University, the United States Naval Observatory, and the University of Washington.

REFERENCES

Akritas, M. G., & Siebert, J. 1996, MNRAS, 919, 924
Anderson, S. F. 1985, PhD Thesis, Washington University, Seattle
Anderson, S. F., & Margon, B. 1987, ApJ, 314, 111
Avni, Y., Soltan, A., Tananbaum, H., & Zamorani, G. 1980, ApJ, 238, 800
Avni, Y., & Tananbaum, H. 1982, ApJ, 262, L17
Avni, Y., & Tananbaum, H. 1986, ApJ, 305, 83
Avni, Y., Worrall, D. M., & Morgan Jr., W. A. 1995, ApJ, 454, 673
Bechtold, J., et al. 2002, ApJ, in press (astro-ph/0204462)
Becker, R. H., White, R. L., & Helfand, D. J. 1995, ApJ, 450, 559
Begelman, M. C. 1978, MNRAS, 184, 53
Blair, A. J., Stewart, G. C., Georgantopoulos, I., Boyle, B. J., Griffiths, R. E., Shanks, T., & Almaini, O. 2000, MNRAS, 314, 138
Boroson, T. A., & Meyers, K. A. 1992, ApJ, 397, 442
Boyle, B. J., Shanks, T., Georgantopoulos, I., Stewart, G. C., & Griffiths, R. E. 1994, MNRAS, 271, 639
Boyle, B. J., Shanks, T., Croom, S. M., Smith, R. J., Miller, L., Loaring, N., & Heymans, C. 2000, MNRAS, 317, 1014
Brandt, W. N., Laor, A., & Wills, B. J. 2000, ApJ, 528, 637
Brandt, W. N., Guainazzi, M., Kaspi, S., Fan, X., Schneider, D. P., Strauss, M. A., Clavel, J., & Gunn, J. E. 2001, AJ, 121, 591
Brandt, W. N., et al. 2002, ApJ, 569, L5

Brown, B. W. M., Hollander, M., & Korwar, R. M. 1974, in Reliability and Biometry, ed. F. Proschan, & R. J. Serfling (Philadelphia: SIAM), 327
Buckley, J., & James, I. 1979, Biometrika, 66, 429
Cappi, M., Matsuoka, M., Comastri, A., Brinkmann, W., Elvis, M., Palumbo, G. G. C., & Vignali, C. 1997, ApJ, 478, 492
Comerford, J. M., Haiman, Z., & Schaye, J. 2002, ApJ, submitted (astro-ph/0206441)
Condon, J. J., Cotton, W. D., Greisen, E. W., Yin, Q. F., Perley, R. A., Taylor, G. B., & Broderick, J. J. 1998, AJ, 115, 1693
Cruddace, R. G., Hasinger, G., & Schmitt, J. H. M. M. 1988, in ESO Conf. and Workshop Proc. 28, Astronomy from large databases: Scientific objectives and methodological approaches, ed. F. Murtagh, & A. Heck (Garching: ESO), 177
Dempster, A. P., Laird, N. M., & Rubin, D. B. 1977, J. Roy. Stat. Soc. B, 39, 1
Dewangan, G. C., Singh, K. P., Gunn, K. F., Newsam, A. M., McHardy, I. M., & Jones, L. R. 2002, MNRAS, in press (astro-ph/0208191)
Dickey, J. M., & Lockman, F. J. 1990, ARA&A, 28, 215
Djorgovski, S. G., Gal, R. R., Odewahn, S. C., de Carvalho, R. R., Brunner, R., Longo, G., & Scaramella, R. 1998, in Wide Field Surveys in Cosmology, ed. S. Colombi, & Y. Mellier (Paris: Editions Frontieres), 89
Fan, X., et al. 1999, ApJ, 526, L57
Fan, X., et al. 2000a, AJ, 119, 1
Fan, X., et al. 2000b, AJ, 120, 1167
Fan, X., et al. 2001a, AJ, 122, 2833
Fan, X., et al. 2001b, AJ, 121, 54
Fasano, G., & Vio, R. 1988, in Newsletter of the Working Group for "Modern Astronomical Methodology", 7, 2
Feigelson, E. D., & Nelson, P. I. 1985, ApJ, 293, 192
Freeman, P. E., Kashyap, V., Rosner, R., & Lamb, D. Q. 2002, ApJS, 138, 185
Fukugita, M., Ichikawa, T., Gunn, J. E., Doi, M., Shimasaku, K., & Schneider, D. P. 1996, AJ, 111, 1748
Gallagher, S. C., Brandt, W. N., Laor, A., Elvis, M., Mathur, S., Wills, B. J., & Iyomoto, N. 2001, ApJ, 546, 795
Gallagher, S. C., Brandt, W. N., Chartas, G., & Garmire, G. P. 2002, ApJ, 567, 37
Garmire, G. P., Bautz, M. W., Ford, P. G., Nousek, J. A., & Ricker, G. R. 2002, Proc. SPIE, 4851, in press
George, I. M., Turner, T. J., Yaqoob, T., Netzer, H., Laor, A., Mushotzky, R. F., Nandra, K., & Takahashi, T. 2000, ApJ, 531, 52
Giommi, P., Angelini, L., Jacobs, P., & Tagliaferri, G. 1992, in ASP Conf. Ser. 25, Astronomical Data Analysis Software and Systems I, ed. D. M. Worrall, C. Biemesderfer, & J. Barnes (San Francisco: ASP), 100
Goodrich, R. W., et al. 2001, ApJ, 561, L23
Green, P. J., et al. 1995, ApJ, 450, 51
Green, P. J., Aldcroft, T. L., Mathur, S., Wilkes, B. J., & Elvis, M. 2001, ApJ, 558, 109
Gunn, J. E., et al. 1998, AJ, 116, 3040
Hasinger, G., Burg, R., Giacconi, R., Schmidt, M., Trumper, J., & Zamorani, G. 1998, A&A, 329, 482
Hewett, P. C., Foltz, C. B., & Chaffee, F. H. 1995, AJ, 109, 1498
Isobe, T., Feigelson, E. D., & Nelson, P. I. 1986, ApJ, 306, 490
Ivezic, Z., et al. 2002, AJ, 124, 2364
Kauffmann, G., & Haehnelt, M. 2000, MNRAS, 311, 576
Kellermann, K. I., Sramek, R., Schmidt, M., Shaffer, D. B., & Green, R. F. 1989, AJ, 98, 1195
Kembhavi, A., Feigelson, E. D., & Singh, K. P. 1986, MNRAS, 220, 51
Kendall, M. G. 1970, in Rank Correlation Methods, 4^{th} edn. (New York: Hafner)
Kriss, G. A., & Canizares, C. R. 1985, ApJ, 177, 193
La Franca, F., Franceschini, A., Cristiani, S., & Vio, R. 1995, A&A, 299, 19
La Franca, F., et al. 2002, ApJ, 570, 100
Laor, A., & Brandt, W. N. 2002, ApJ, 569, 641
LaValley, M., Isobe, T., & Feigelson, E. D. 1992, in ASP Conf. Ser. 25, Astronomical Data Analysis Software and Systems, ed. D. M. Worrall, C. Biemesderfer, & J. Barnes (San Francisco: ASP), 245
Lightman, A. P., & Eardley, D. M. 1974, ApJ, 187, L1
Lineweaver, C. H. 2001, in COSMO-01: International Workshop on Particle Physics and the Early Universe, in press (astro-ph/0112381)
Maiolino, R., Mannucci, F., Baffa, C., Gennari, S., & Oliva, E. 2001, A&A, 372, L5
Marshall, H. L., Avni, Y., Braccesi, A., Huchra, J. P., Tananbaum, H., Zamorani, G., & Zitelli, V. 1984, ApJ, 283, 50
Mineo, T., et al. 2000, A&A, 359, 471
Miyaji, T., Hasinger, G., & Schmidt, M. 2000, A&A, 353, 25
Mukai, K. 2001, PIMMS Users' Guide (Greenbelt: NASA/GSFC)
Page, K. L., Turner, M. J. L., Reeves, J. N., O'Brien, P. T., & Sembay, S. 2002, MNRAS, in press (astro-ph/0210140)
Pickering, T. E., Impey, C. D., & Foltz, C. B. 1994, AJ, 108, 1542
Rees, M. J. 1978, Phys. Scr, 17, 193
Reeves, J. N., & Turner, M. J. L. 2000, MNRAS, 316, 234
Richards, G. T., et al. 2002, AJ, 123, 2945
Schlegel, D. J., Finkbeiner, D. P., & Davis, M. 1998, ApJ, 500, 525
Schneider, D. P., et al. 2002, AJ, 123, 567
Shakura, N. I., & Sunyaev, R. A. 1976, MNRAS, 175, 613
Stern, D., Djorgovski, S. G., Perley, R. A., de Carvalho, R. R., & Wall, J. V. 2000, AJ, 119, 1526
Stoughton, C., et al. 2002, AJ, 123, 485
Tananbaum, H., Avni, Y., Green, R. F., Schmidt, M., & Zamorani, G. 1986, ApJ, 305, 57
Tolea, A., Krolik, J. H., & Tsvetanov, Z. 2002, ApJ, 578, L31
Turnshek, D. A., Monier, E. M., Sirola, C. J., & Espey, B. R. 1997, ApJ, 476, 40
Vanden Berk, D. E., et al. 2001, AJ, 122, 549
Vignali, C., Comastri, A., Cappi, M., Palumbo, G. G. C., Matsuoka, M., & Kubo, H. 1999, ApJ, 516, 582
Vignali, C., Brandt, W. N., Fan, X., Gunn, J. E., Kaspi, S., Schneider, D. P., & Strauss, M. A. 2001a, AJ, 122, 2143
Vignali, C., Comastri, A., Fiore, F., & La Franca, F., 2001b, A&A, 370, 900
Vignali, C., Brandt, W. N., Schneider, D. P., Garmire, G. P., & Kaspi, S. 2003, AJ, in press (astro-ph/0210475)
Voges, W., et al. 1999, A&A, 349, 389
Weymann, R. J., Morris, S. L., Foltz, C. B., & Hewett, P. C. 1991, ApJ, 373, 23
Wyithe, S., & Loeb, A. 2002, Nature, 417, 923
Wilkes, B. J., & Elvis, M. 1987, ApJ, 323, 243
Wilkes, B. J., Tananbaum, H., Worrall, D. M., Avni, Y., Oey, M. S., & Flanagan, J. 1994, ApJS, 92, 53
Worrall, D. M., Tananbaum, H., Giommi, P., & Zamorani, G. 1987, ApJ, 313, 596
York, D. G., et al. 2000, AJ, 120, 1579
Yuan, W., Brinkmann, W., Siebert, J., & Voges, W. 1998a, A&A, 330, 108
Yuan, W., Siebert, J., & Brinkmann, W. 1998b, A&A, 334, 498
Zamorani, G., et al. 1981, ApJ, 245, 357
Zimmermann, H. U., Boese, G., Becker, W., Belloni, T., Döbereiner, S., Izzo, C., Kahabka, P., & Schwentker, O. 1998, EXSAS User's Guide, MPE Report, *ROSAT* Scientific Data Center

TABLE 2

PROPERTIES OF THE SDSS QUASARS WITH X-RAY OBSERVATIONS

SDSS Object	Alt. Name[a]	z	$AB_{1450(1+z)}$	M_B	$f_{2500\,Å}$[b]	$\log L_{2500\,Å}$[c]	$f_{0.5-2\,\mathrm{keV}}$[d]	$f_{2\,\mathrm{keV}}$[b]	$\log L_{2\,\mathrm{keV}}$[c]	α_{ox}	$f_{1.4\,\mathrm{GHz}}$[e]	R[f]	Instr.[g]	Exp.[h]	Off-Axis[i]	Obs. ID
000710.01+005329.0	LBQS 0004+0036	0.316	17.67	−23.95	5.07	30.10	8.85	1.74	26.63	−1.330	1.55	0.93	R	396		rs931701n00
000834.71+003156.1	LBQS 0006+0015	0.263	18.26	−22.70	2.94	29.70	3.21	0.604	26.01	−1.415	< 0.44	< 0.56	R	395		rs931701n00
001257.25+011527.3		0.504	18.90	−23.31	1.59	30.02	3.21	0.721	26.67	−1.284	< 0.36	< 1.14	R	384		rs931701n00
002209.95+001629.3	LBQS 0019-0000	0.575	18.58	−24.05	2.22	30.28	2.99	0.703	26.78	−1.343	< 1.34	< 2.95	R	401		rs931701n00
002303.14+011533.6	LBQS 0020+0058	0.728	18.57	−24.60	2.31	30.50	2.92	0.754	27.02	−1.338	< 0.39	< 0.89	R	426		rs931702n00
002311.06+003517.4	LBQS 0020+0018	0.422	20.24	−22.08	0.47	29.33	3.05	0.647	26.46	−1.100	< 0.50	< 3.27	R	408		rs931702n00
003242.74+003110.8		0.361	18.79	−22.76	1.81	29.77	4.07	0.826	26.43	−1.282	< 0.41	< 1.00	R	610		rs931702n00
003333.61−001858.1		0.690	19.56	−23.80	1.06	30.12	5.21	1.31	27.21	−1.116	< 0.45	< 1.91	R	626		rs931702n00
003340.21−005525.6		0.937	18.23	−25.56	3.28	30.88	3.74	1.08	27.39	−1.337	< 0.45	< 0.79	R	635		rs931702n00
003431.74−001312.7		0.381	18.63	−23.25	2.09	29.88	2.69	0.055	25.30	−1.757	< 0.41	< 0.73	R	571		rs931702n00
004319.74+005115.4	UM 269	0.308	18.55	−22.58	2.26	29.72	4.62	0.901	26.32	−1.305	1.60	3.22	R	320		rs931702n00
004613.53+010425.7†	UM 275	2.152	18.36	−27.29	3.31	31.56	< 0.131	< 0.062	< 26.83	< −1.816	3.04	7.58	P	10718	0.0	rp700377n00
004704.46+005228.2		1.620	18.74	−25.95	1.57	31.01	0.362	0.142	26.97	−1.553	< 0.38	< 1.65	P	10718	17.2	rp700377n00
005121.25+004521.6	LBQS 0048+0029	0.727	18.91	−24.52	1.67	30.36	< 0.347	< 0.089	< 26.09	< −1.640	< 0.43	< 1.07	H	12142	19.4	rh701865n00
005202.40+010129.1	LBQS 0049+0045	2.272	17.46	−28.09	5.75	31.84	< 0.436	< 0.213	< 27.41	< −1.702	< 0.28	< 0.38	H	12142	0.0	rh701865n00
005235.25+010227.9		1.390	18.79	−25.84	1.87	30.97	< 0.289	< 0.103	< 26.71	< −1.635	< 0.25	< 0.86	H	12142	8.2	rh701865n00
005441.19+000110.6	LBQS 0052-0015	0.647	18.60	−24.44	2.14	30.37	4.50	1.11	27.08	−1.262	3.08	6.25	R	371		rs931703n00
010226.32−003904.5	DMS 0059-0055	0.294	16.78	−24.33	11.5	30.39	7.10	1.37	26.47	−1.506	< 0.46	< 0.17	R	393		rs931703n00
010603.86+010506.2		1.611	19.33	−25.64	1.17	30.88	< 0.647	< 0.252	< 27.21	< −1.407	< 0.44	< 2.57	H	12672	11.7	rh703871n00
010614.39+011409.3		1.356	19.69	−24.88	0.79	30.57	< 0.312	< 0.110	< 26.71	< −1.480	< 0.41	< 3.21	H	12672	13.9	rh703871n00
010648.02+004627.8	LBQS 0104+0030	1.883	18.59	−26.49	1.91	31.22	< 0.364	< 0.157	< 27.13	< −1.568	< 0.45	< 1.71	H	12672	17.1	rh703871n00
011254.91+000313.0	PB 06317	0.239	18.08	−22.49	3.47	29.68	5.89	1.09	26.18	−1.345	< 0.45	< 0.56	R	419		rs931704n00
011757.79−010809.9		0.707	19.27	−23.62	1.18	30.19	1.04	0.266	26.54	−1.400	< 0.48	< 2.57	H	16618	15.9	rh702758a01
011758.83+002021.4		0.613	19.02	−23.69	1.55	30.18	4.47	1.07	27.02	−1.212	< 0.41	< 1.47	R	406		rs931704n00
011817.10−011421.9		0.668	19.94	−23.27	0.63	29.86	< 0.288	< 0.072	< 25.92	< −1.513	< 0.47	< 3.02	H	16618	16.9	rh702758a01
011824.29−010832.0		0.967	19.35	−24.21	0.96	30.37	< 0.296	< 0.087	< 26.33	< −1.552	< 0.49	< 3.17	H	16618	11.1	rh702758a01
011827.98−005239.8	UM 314	2.190	18.30	−27.17	2.75	31.49	0.319	0.152	27.24	−1.634	< 0.42	< 1.22	H	16618	9.7	rh702758a01
011855.75−004032.4		0.745	18.66	−24.16	1.92	30.44	< 0.292	< 0.076	< 26.04	< −1.690	< 0.44	< 1.61	H	16618	19.5	rh702758a01
011922.85−004419.8	NGC 0450:[GMS97] 120	1.054	18.68	−25.40	2.00	30.76	1.49	0.456	27.12	−1.398	< 0.43	< 1.14	H	16618	17.5	rh702758a01
012602.20−001924.1	NGC 0450:[GMS97] 099	1.761	18.81	−26.36	1.81	31.14	0.213	0.088	26.83	−1.657	< 2.12	< 7.77	P	13057	11.0	rp800645n00
013041.65+004000.2		0.655	18.47	−24.42	2.49	30.44	3.30	0.815	26.96	−1.338	< 0.47	< 0.99	R	430		rs931705n00
013418.18+001536.7	UM 341	0.399	17.13	−24.73	8.33	30.52	12.2	2.54	27.01	−1.349	< 0.61	< 0.30	R	386		rs931705n00
014017.07−005002.9	UM 357	0.335	16.70	−24.67	12.4	30.54	2.12	4.23	27.07	−1.331	< 0.45	< 0.16	R	230		rs931705n00
014544.09−003828.9†		1.851	20.05	−25.53	0.74	30.79	< 0.338	< 0.144	< 27.08	< −1.424	< 0.44	< 3.93	P	6032	13.7	rp701219n00
014618.05−005131.9		0.832	19.07	−24.53	1.47	30.42	< 0.264	< 0.072	< 26.12	< −1.654	< 0.45	< 1.52	P	6032	12.4	rp701219n00
014619.97−004628.8	UM 368	3.175	19.02	−27.10	1.32	31.45	0.139	0.087	27.26	−1.605	< 0.43	< 3.07	P	6032	7.8	rp701219n00
014705.43−004148.9†		2.108	20.46	−26.15	1.00	31.02	< 0.206	< 0.096	< 27.01	< −1.543	< 0.44	< 2.97	P	6032	6.9	rp701219n00
014942.50+001501.7		0.552	16.81	−25.68	11.4	30.95	6.21	1.44	27.05	−1.497	< 0.41	< 0.18	R	434		rs931705n00
015248.42+011442.7		1.171	19.15	−25.01	1.23	30.64	< 0.431	< 0.140	< 26.70	< −1.515	< 0.45	< 2.18	H	15850	14.2	rh800731n00
015258.67+010507.3		0.646	19.79	−23.09	0.72	29.89	0.427	0.105	26.06	−1.473	< 0.43	< 2.99	H	15850	6.3	rh800731n00
015309.13+005250.1		1.162	19.60	−24.81	0.97	30.53	< 0.314	< 0.101	< 26.55	< −1.528	< 0.46	< 2.63	H	15850	10.5	rh800731n00
015906.38+002343.9		2.321	19.30	−26.33	1.10	31.14	< 0.201	< 0.099	< 27.09	< −1.552	< 0.46	< 3.28	P	6155	11.0	rp700225n00
015910.05+010514.5		0.217	18.04	−22.56	3.61	29.61	5.12	0.931	26.02	−1.378	< 0.44	< 0.41	R	409		rs931706n00
015935.48+000401.2		3.278	20.05	−26.06	0.53	31.07	< 0.267	< 0.170	< 27.58	< −1.339	< 0.42	< 8.49	P	6155	19.7	rp700225n00
015938.08+002639.2		1.606	18.88	−25.90	1.48	30.98	< 0.284	< 0.111	< 26.85	< −1.584	< 0.42	< 1.89	P	6155	4.5	rp700225n00
015945.92+000521.4		0.389	19.18	−22.61	1.26	29.68	1.47	0.305	26.06	−1.388	< 0.42	< 1.39	P	6155	18.1	rp700225n00
015950.24+002340.8	MRK 1014	0.163	16.18	−23.40	20.0	30.10	9.87	1.71	26.03	−1.562	24.08	5.56	P	6155	0.0	rp700225n00
020047.38+003110.1		1.620	18.45	−26.21	1.97	31.11	0.463	0.181	27.08	−1.550	< 0.45	< 1.57	P	6155	16.2	rp700225n00
020115.53+003135.1		0.362	18.60	−22.90	2.16	29.85	4.25	0.863	26.45	−1.304	< 0.43	< 0.92	P	1644	3.4	rp700972n00
021102.72−000910.3		4.900	20.00	−26.85	0.48	31.30	0.031	0.027	27.06	−1.628	< 0.44	< 10.35	C	4888	0.0	700271
021359.78+004226.7		0.182	18.14	−21.94	3.30	29.41	12.0	2.12	26.22	−1.226	3.90	4.39	R	235		rs931706n00
021425.69−003859.7		1.726	18.06	−26.73	2.88	31.33	< 0.543	< 0.221	< 27.21	< −1.580	< 0.46	< 1.14	P	3484	7.4	rp701229n00
021449.10−005040.9		1.603	19.37	−25.30	0.86	30.74	< 0.501	< 0.195	< 27.10	< −1.400	< 0.41	< 3.16	P	3484	5.9	rp701229n00
021457.21−010323.9		1.770	19.53	−25.60	0.94	30.86	< 0.503	< 0.208	< 27.21	< −1.403	< 0.45	< 3.35	P	3484	18.2	rp701229n00
023325.33+002914.8		2.014	18.45	−26.76	2.29	31.35	0.381	0.172	27.22	−1.583	< 0.43	< 1.48	P	28216	16.1	rp800482n00
023333.23+010333.0		2.060	18.58	−26.80	2.09	31.33	< 0.108	< 0.049	< 26.70	< −1.777	< 0.45	< 1.59	P	28216	18.6	rp800482n00
023359.71+004938.5		2.523	17.78	−27.88	4.37	31.80	0.286	0.151	27.34	−1.713	< 0.45	< 0.92	P	28216	6.6	rp800482n00
024141.52+000416.5	[CLA95] 023907.70-00	0.648	18.83	−23.85	1.63	30.25	0.470	0.116	26.10	−1.593	< 1.19	< 4.14	P	5471	15.5	rp150021a02
024240.31+005727.1	E 0240+007	0.569	16.74	−25.82	12.2	31.01	0.164	3.85	27.51	−1.343	3.58	1.50	R	234		rs931708n00
024304.68+000005.4†	[CLA95] 024030.91-00	2.003	18.53	−26.85	2.51	31.38	0.220	0.099	26.98	−1.691	< 1.25	< 3.95	P	5471	6.0	rp150021a02
024441.42+011434.4		0.546	20.09	−23.03	0.75	29.76	1.34	0.308	26.37	−1.299	< 0.42	< 2.10	H	27741	17.4	rh600999n00
025331.93+001624.7†	[LCB92] 0250+0004	1.825	19.01	−26.03	1.34	31.04	< 0.606	< 0.255	< 27.32	< −1.428	< 0.44	< 2.40	P	2949	19.8	rp190332n00
025356.07+001057.3	[LCB92] 0251-0001B	1.699	19.29	−25.55	0.99	30.85	< 0.607	< 0.245	< 27.24	< −1.385	< 0.44	< 3.08	P	2949	13.0	rp190332n00
025438.36+002132.6		2.465	19.73	−26.14	0.83	31.06	0.081	0.042	26.76	−1.650	< 0.44	< 4.25	P	11855	13.4	rp701403n00
025505.66+002523.0	US 3333	0.354	17.94	−23.38	3.96	30.09	4.69	0.948	26.47	−1.390	< 0.45	< 0.60	P	11855	14.7	rp701403n00
025513.02+000639.4	[LCB92] 0252-0005	1.886	19.12	−25.84	1.05	30.96	0.309	0.133	27.06	−1.495	< 0.42	< 2.92	P	11855	4.2	rp701403n00
025518.58+004847.4		3.990	18.76	−27.80	1.91	31.77	< 1.46	< 1.080	< 28.52	< −1.246	< 0.45	< 2.80	P	850	14.1	rp190035n00
025559.92+005311.4	[HB89] 0253+006	0.846	18.71	−24.72	1.97	30.57	< 1.56	< 0.429	< 26.90	< −1.406	< 0.46	< 1.35	P	850	11.4	rp190035n00
025607.24+011038.6	[LCB92] 0253+0058	1.349	19.19	−25.59	1.45	30.83	< 1.76	< 0.618	< 27.46	< −1.294	< 0.45	< 1.78	P	850	11.9	rp190035n00
025702.08−010217.2	[LCB92] 0254-0114	0.874	19.32	−24.14	1.01	30.31	0.340	0.095	26.28	−1.546	< 0.45	< 2.42	P	2996	11.6	rp190338n00
025705.87−001053.5	[LCB92] 0254-0022	1.586	19.43	−25.48	1.03	30.81	< 1.29	< 0.498	< 27.50	< −1.272	< 0.44	< 2.86	P	949	11.4	rp190037n00
025713.07−010157.8	[CLB91] 025440.2-011	1.869	19.31	−25.82	1.02	30.94	0.753	0.322	27.44	−1.343	< 0.45	< 3.13	P	2996	13.6	rp190338n00
025717.35−011413.0		1.924	19.36	−25.78	0.95	30.93	< 0.698	< 0.305	< 27.44	< −1.342	< 0.43	< 3.27	P	1996	10.6	rp190338n00
025735.33−001631.4		0.362	20.45	−21.91	0.39	29.11	< 1.30	< 0.264	< 25.94	< −1.218	< 0.45	< 2.43	P	949	6.2	rp190037n00
025743.73+011144.4		1.705	19.25	−25.84	1.34	30.99	< 1.21	< 0.490	< 27.55	< −1.320	< 0.45	< 2.47	P	986	17.8	rp190328n00
025751.55+002045.4	[HB89] 0255+001	1.500	19.81	−25.24	0.88	30.70	< 0.401	< 0.150	< 26.93	< −1.447	< 0.44	< 3.14	P	2894	7.3	rp190330n00
025815.54−000334.2	US 3437	1.319	19.26	−25.21	1.12	30.70	< 0.488	< 0.169	< 26.88	< −1.467	< 0.44	< 2.33	P	4984	19.4	rp700393n00
025905.64+001121.9	LBQS 0256-0000	3.366	17.63	−28.61	5.01	32.07	0.960	0.625	28.16	−1.499	2.59	5.29	P	4984	0.0	rp700393n00
025922.64+005829.4	US 3461	1.861	18.63	−26.47	1.95	31.22	< 1.19	< 0.508	< 27.63	< −1.375	< 0.45	< 1.68	P	986	19.8	rp190328n00
030027.11−004848.8	US 3499	2.015	18.86	−26.41	1.58	31.19	< 0.958	< 0.431	< 27.62	< −1.369	< 0.43	< 2.06	P	1801	10.6	rp190340n00
030035.97−001533.0	[LCB92] 0258-0027	1.446	18.69	−25.76	1.70	30.96	< 0.826	< 0.301	< 27.20	< −1.440	< 0.71	< 2.86	P	1814	10.8	rp190334n00
030100.23+000429.2		0.486	19.64	−22.71	0.85	29.71	< 0.709	< 0.157	< 25.98	< −1.434	< 0.44	< 2.25	P	1814	10.6	rp190334n00
030335.76+004144.8		0.669	20.24	−23.57	0.58	29.83	< 0.340	< 0.085	< 25.99	< −1.472	< 0.45	< 2.19	P	5584	18.4	rp700395n00

TABLE 2—*Continued*

SDSS Object	Alt. Name[a]	z	$AB_{1450(1+z)}$	M_B	$f_{2500\,Å}$[b]	$\log L_{2500\,Å}$[c]	$f_{0.5-2\,\mathrm{keV}}$[d]	$f_{2\,\mathrm{keV}}$[b]	$\log L_{2\,\mathrm{keV}}$[c]	α_{ox}	$f_{1.4\,\mathrm{GHz}}$[e]	R[f]	Instr.[g]	Exp.[h]	Off-Axis[i]	Obs. ID
030342.79+002700.5	LBQS 0301+0015	1.651	18.00	−26.92	3.66	31.40	0.466	0.184	27.10	−1.650	< 0.44	< 0.83	P	5584	3.8	rp700395n00
030422.39+002231.7	LBQS 0301+0010	0.638	17.27	−25.57	7.31	30.89	0.173	0.042	25.65	−2.011	< 0.43	< 0.30	P	5584	10.3	rp700395n00
103027.10+052455.0		6.280	19.66	−27.59	0.65	31.60	0.020	0.021	27.11	−1.723	< 0.46	< 9.32	C	7956	0.0	700605
103457.28−010209.0		0.328	18.37	−23.20	2.66	29.85	4.04	0.801	26.33	−1.352	< 0.43	< 0.56	R	385		rs931729n00
103709.80+000235.1		2.681	20.30	−25.75	0.53	30.92	< 0.145	< 0.080	< 27.11	< −1.466	< 0.46	< 7.85	P	18097	11.1	rp201243n00
103747.41−001643.9		1.498	20.00	−25.21	0.85	30.68	< 0.183	< 0.068	< 26.59	< −1.572	< 0.42	< 3.07	P	18097	13.5	rp201243n00
104152.61−001102.1†	2QZ J104152.5-001102	1.703	19.45	−25.58	0.94	30.83	< 0.203	< 0.082	< 26.77	< −1.559	< 0.45	< 3.14	P	7202	11.2	rp800194n00
104159.13−001126.3	2QZ J104159.0-001127	0.794	19.76	−23.93	0.75	30.09	0.516	0.138	26.36	−1.433	< 0.45	< 2.37	P	7202	9.6	rp800194n00
104243.13−001706.0		1.972	18.27	−27.01	2.85	31.43	0.225	0.100	26.97	−1.711	< 0.46	< 1.20	P	7202	2.7	rp800194n00
104253.44−001300.8		2.957	18.89	−27.18	1.58	31.48	0.296	0.174	27.52	−1.520	< 0.45	< 2.55	P	7202	5.5	rp800194n00
104433.04−012502.2†		5.745	19.21	−27.90	0.98	31.72	0.012	0.012	26.81	−1.886	< 0.45	< 5.72	X	32613	0.0	0125300101
104552.42+002410.2		0.556	18.96	−23.53	1.60	30.11	3.56	0.827	26.82	−1.262	< 0.47	< 1.52	R	405		rs931729n00
105336.71−001727.3	2QZ J105336.6-001727	0.482	19.55	−22.56	0.88	29.72	0.750	0.166	25.99	−1.429	< 0.45	< 2.59	P	4732	4.0	rp700381n00
105337.95+005958.8		0.476	19.64	−22.69	0.85	29.69	3.42	0.754	26.64	−1.172	< 0.44	< 2.19	R	416		rs931730n00
105338.37−002804.4	2QZ J105338.3-002805	1.840	18.81	−26.28	1.65	31.14	< 0.478	< 0.203	< 27.23	< −1.501	< 0.42	< 1.85	P	4732	12.0	rp700381n00
105414.10−001803.6	2QZ J105414.1-001804	1.163	19.39	−24.87	1.05	30.57	< 0.309	< 0.100	< 26.54	< −1.544	< 0.44	< 2.39	P	4732	13.2	rp700381n00
110057.71−005304.5		0.378	17.80	−23.75	4.49	30.21	6.31	1.30	26.67	−1.359	< 0.52	< 0.57	R	433		rs931730n00
112405.48+002401.9		0.789	19.35	−24.48	1.17	30.28	3.13	0.836	27.13	−1.208	< 0.42	< 1.30	R	421		rs931731n00
112956.10−014212.4†		4.850	19.20	−27.63	0.97	31.62	< 0.020	< 0.017	< 26.85	< −1.829	< 0.41	< 4.65	C	4818	0.0	700272
113541.20+002235.2	[VCV96] Q 1133+0039	0.175	18.11	−21.81	3.39	29.39	4.94	0.865	25.80	−1.379	< 0.42	< 0.49	R	427		rs931731n00
114612.09+002105.1	2QZ J114612.0+002104	1.229	19.19	−25.03	1.21	30.67	0.343	0.114	26.65	−1.545	< 0.49	< 2.63	P	5837	10.2	rp201242n00
114647.72+001350.6	LBQS 1144+0030	0.940	18.22	−25.47	2.95	30.83	0.719	0.208	26.68	−1.594	< 0.43	< 0.82	P	5837	3.1	rp201242n00
114733.67+000811.5	2QZ J114733.6+000811	1.077	19.55	−24.54	0.89	30.43	0.586	0.182	26.74	−1.416	< 0.46	< 2.82	P	5837	15.1	rp201242n00
115758.73−002220.8		0.260	17.38	−23.46	6.61	30.04	2.64	0.497	25.91	−1.583	< 0.46	< 0.28	R	359		rs931732n00
120014.08−004638.7		0.179	18.48	−21.66	2.41	29.26	11.1	1.96	26.17	−1.186	< 0.44	< 0.61	R	366		rs931733n00
120441.73−002149.6		5.030	19.10	−27.79	1.09	31.68	0.038	0.034	27.17	−1.730	< 0.45	< 4.69	C	6272	0.0	700373
120823.82+001027.7		5.273	20.50	−26.47	0.30	31.15	0.011	0.010	26.69	−1.713	< 0.46	< 18.05	C	4619	0.0	700273
123514.95+004740.7		1.876	19.92	−25.70	0.86	30.87	< 0.180	< 0.077	< 26.82	< −1.554	< 0.48	< 3.71	P	23511	18.6	rp700355n00
123552.74+005029.6		2.241	19.29	−26.26	1.10	31.11	0.078	0.378	27.65	−1.329	< 0.42	< 2.95	P	23511	8.8	rp700355n00
123659.89+004212.1	2QZ J123659.9+004211	2.378	19.06	−26.47	1.32	31.24	0.177	0.089	27.07	−1.601	< 0.44	< 2.94	P	23511	15.3	rp700355n00
123724.52+010615.5	LBQS 1234+0122	2.023	18.23	−27.17	3.02	31.47	< 0.303	< 0.049	< 26.68	< −1.840	< 0.42	< 1.01	P	23511	19.1	rp700355n00
123729.74+005433.6		3.279	18.99	−27.26	1.45	31.51	0.201	0.109	27.39	−1.583	< 0.46	< 3.03	P	23511	16.4	rp700355n00
124540.99−002744.9	LBQS 1243-0011	1.687	18.98	−26.23	1.72	31.08	1.01	0.407	27.46	−1.392	< 0.48	< 1.80	P	16761	7.8	rp600532n00
124555.12−003735.5	2QZ J124555.1-003736	1.042	18.94	−24.92	1.50	30.63	0.482	0.147	26.62	−1.539	< 0.45	< 1.82	P	16761	15.2	rp600532n00
130018.84+000756.5		1.305	20.36	−25.18	0.82	30.56	< 0.309	< 0.106	< 26.67	< −1.493	< 0.43	< 2.30	H	7247	0.9	rh201701n00
130608.26+035626.3		5.990	19.55	−27.62	0.72	31.61	0.044	0.046	27.42	−1.611	< 0.41	< 7.24	C	8158	0.0	700606
130713.25−003601.7		0.170	17.96	−21.78	3.89	29.43	7.78	1.36	25.97	−1.327	< 0.41	< 0.46	R	251		rs931735n00
131131.03−010332.3		1.304	18.94	−25.49	1.50	30.82	< 0.150	< 0.052	< 26.35	< −1.714	< 0.48	< 1.93	P	13949	16.9	rp800248n00
131208.68−010710.1		0.805	19.61	−23.78	0.87	30.17	0.602	0.162	26.44	−1.432	< 0.47	< 2.89	P	13949	16.1	rp800248n00
132020.27−003428.2	LBQS 1317-0018	0.353	18.94	−22.52	1.58	29.69	3.86	0.780	26.39	−1.269	< 0.70	< 2.04	R	273		rs931736n00
134044.52−004516.6	LBQS 1338-0030	0.384	17.63	−23.97	5.25	30.29	2.99	0.618	26.36	−1.509	< 0.43	< 0.40	R	310		rs931737n00
134113.93−005315.0	LBQS 1338-0038	0.237	18.15	−22.42	3.25	29.65	6.06	1.12	26.18	−1.330	5.38	6.96	R	343		rs931737n00
134233.70−001148.1	2QZ J134233.7-001148	0.516	19.67	−22.73	0.85	29.76	0.213	0.048	25.52	−1.630	< 0.47	< 2.69	P	27254	17.6	rp701000a01
134256.51+000057.2	F864:072	0.804	19.48	−23.84	1.00	30.23	1.29	0.347	26.77	−1.328	< 0.47	< 2.74	P	27254	19.5	rp701000a01
134325.84−001612.2	2QZ J134325.8-001612	1.514	19.45	−25.40	1.01	30.77	< 0.084	< 0.032	< 26.26	< −1.729	< 0.42	< 2.64	P	27254	4.5	rp701000a01
134425.94−000056.2		1.097	18.99	−24.92	1.37	30.63	0.253	0.079	26.39	−1.627	< 0.44	< 2.01	P	27254	17.7	rp701000a01
134459.44−001559.5	LBQS 1342-0000	0.245	18.21	−22.48	3.08	29.65	2.06	0.383	25.75	−1.499	< 0.45	< 0.60	P	21103	14.6	rp800369a01
134507.93−001900.9		0.419	20.61	−22.48	0.34	29.18	0.370	0.078	25.54	−1.395	< 0.44	< 1.95	P	5048	17.8	rp800369n00
135128.32+010338.5	LBQS 1348+0118	1.085	17.65	−26.51	5.57	31.23	3.82	1.19	27.56	−1.409	< 0.47	< 0.48	R	377		rs931737n00
141637.44+003352.2	2QZ J141637.4+003351	0.434	19.77	−22.60	0.74	29.55	3.64	0.779	26.57	−1.143	< 0.41	< 1.78	R	404		rs931739n00
142441.21−000727.2		0.318	19.13	−22.50	1.32	29.52	8.36	1.64	26.61	−1.115	< 0.45	< 1.06	R	336		rs931739n00
142658.57−002056.4	EQS B1424-0007	0.627	17.24	−25.52	7.91	30.91	4.10	0.995	27.01	−1.497	< 0.42	< 0.29	R	328		rs931739n00
143143.80−005011.4	LBQS 1429-0036	1.190	18.59	−25.84	2.46	30.96	< 0.146	< 0.048	< 26.24	< −1.809	< 0.55	< 1.29	H	33627	19.4	rh800679n00
152241.31−004214.9		1.081	19.59	−24.84	1.05	30.51	< 2.11	< 0.655	< 27.30	< −1.231	< 0.41	< 1.93	H	1434	16.9	rh701907n00
152316.31−004150.5		0.444	18.62	−23.28	2.15	30.03	< 1.57	< 0.337	< 26.23	< −1.460	< 0.45	< 1.09	H	1434	8.5	rh701907n00
152348.99−004701.8†		3.293	18.61	−27.77	2.40	31.73	< 2.10	< 1.34	< 28.48	< −1.248	< 0.41	< 1.74	H	1434	2.0	rh701907n00
153259.96−003944.1		4.620	19.40	−27.35	0.83	31.50	< 0.020	< 0.017	< 26.82	< −1.797	< 0.45	< 5.92	C	5087	0.0	700275
160501.21−011220.0†		4.920	19.40	−27.46	0.83	31.55	< 0.020	< 0.018	< 26.87	< −1.793	< 0.45	< 6.17	C	4641	0.0	700276
165338.68+634010.5		0.279	18.51	−22.55	2.34	29.65	0.826	0.158	25.48	−1.601	< 1.50	< 2.48	R	2839		rs930624n00
165537.78+624739.0		0.597	19.50	−23.49	0.98	29.96	0.453	0.108	26.00	−1.519	< 1.50	< 6.00	P	17735	18.1	rp900169n00
165627.31+623226.8		0.185	18.73	−21.63	1.91	29.19	0.186	0.033	24.43	−1.829	< 1.50	< 2.33	P	17735	5.3	rp900169n00
165951.98+622758.6		1.325	19.41	−24.98	0.91	30.61	< 0.181	< 0.063	< 26.45	< −1.598	< 1.50	< 10.10	P	17735	19.1	rp900169n00
165958.93+620218.1		0.232	18.37	−22.19	2.65	29.54	1.41	0.259	25.53	−1.539	< 1.50	< 2.29	R	1975		rs930624n00
170049.55+643159.3		1.258	18.84	−25.23	1.39	30.75	0.362	0.122	26.70	−1.557	< 1.50	< 7.10	P	16073	19.9	rp701121n00
170113.94+635243.0		1.762	18.08	−26.76	2.81	31.33	0.211	0.087	26.82	−1.731	< 1.50	< 3.80	P	27387	19.3	rp701457n00
170406.14+604753.7	CRSS J1704.1+6047	1.364	18.68	−25.80	1.71	30.91	0.724	0.255	27.09	−1.469	< 1.50	< 5.05	P	15372	5.6	rp701439n00
170438.97+585748.7		0.918	19.25	−24.75	1.47	30.51	1.61	0.462	27.01	−1.344	< 1.50	< 5.22	R	1160		rs930728n00
170441.37+604430.4	[HB89] 1704+608	0.372	16.13	−25.77	21.0	30.86	4.30	0.881	26.49	−1.680	< 1.50	< 0.24	P	15372	0.0	rp701439n00
170611.40+610052.9		2.061	19.36	−26.05	1.10	31.05	< 0.249	< 0.114	< 27.06	< −1.530	< 1.50	< 10.53	P	15372	19.8	rp701439n00
170817.87+615448.6		1.419	18.53	−26.38	2.54	31.11	1.26	0.456	27.37	−1.438	< 1.50	< 3.25	R	1808		rs930624n00
170839.83+652137.7		1.397	18.60	−25.81	1.91	30.98	0.636	0.228	27.05	−1.506	< 1.50	< 5.29	R	3171		rs930521n00
170918.26+622516.1		1.406	19.15	−25.57	1.35	30.83	0.684	0.245	27.09	−1.436	< 1.50	< 6.73	R	2079		rs930624n00
170930.80+641002.9		1.592	18.64	−26.24	1.97	31.10	0.721	0.277	27.25	−1.479	< 1.50	< 4.86	R	3337		rs930624n00
170937.63+640615.0		1.119	18.85	−25.01	1.32	30.63	0.156	0.049	26.21	−1.699	< 1.50	< 6.55	P	14534	18.5	rp800512n00
170956.01+573225.4		0.522	19.06	−23.58	1.51	30.02	2.14	0.487	26.53	−1.340	< 0.43	< 1.15	R	1612		rs930728n00
171007.50+641240.9		1.376	18.25	−26.23	2.60	31.10	0.767	0.272	27.12	−1.528	< 1.50	< 3.47	P	14534	17.9	rp800512n00
171009.85+642256.7		0.256	19.93	−21.70	0.63	29.00	0.599	0.112	25.25	−1.439	< 1.50	< 4.48	R	3498		rs930624n00
171015.72+634806.1		1.786	19.32	−25.70	1.01	30.90	0.659	0.274	27.33	−1.369	< 1.50	< 10.41	R	3194		rs930624n00
171022.61+640602.9		1.248	18.89	−25.55	1.72	30.84	0.162	0.054	26.34	−1.727	< 1.50	< 5.19	P	14534	13.8	rp800512n00
171117.66+584123.7		0.616	19.46	−23.67	1.09	30.03	0.731	0.176	26.24	−1.456	< 0.43	< 1.57	P	7902	11.1	rp900171n00
171126.94+585544.2		0.537	19.54	−22.97	0.93	29.84	0.592	0.136	26.00	−1.473	< 1.50	< 7.57	P	7902	7.7	rp900171n00
171127.49+641722.4		0.798	19.37	−23.84	1.07	30.25	0.710	0.191	26.50	−1.440	< 1.50	< 8.63	P	14534	15.3	rp800512n00
171144.82+584919.6		1.532	19.29	−25.39	0.99	30.77	< 0.133	< 0.050	< 26.47	< −1.648	< 1.50	< 9.71	P	7902	3.4	rp900171n00

TABLE 2—*Continued*

SDSS Object	Alt. Name[a]	z	$AB_{1450(1+z)}$	M_B	$f_{2500\,Å}$[b]	$\log L_{2500\,Å}$[c]	$f_{0.5-2\,\mathrm{keV}}$[d]	$f_{2\,\mathrm{keV}}$[b]	$\log L_{2\,\mathrm{keV}}$[c]	α_{ox}	$f_{1.4\,\mathrm{GHz}}$[e]	R[f]	Instr.[g]	Exp.[h]	Off-Axis[i]	Obs. ID
171207.44+584754.5		0.269	18.55	−22.32	2.25	29.60	2.88	0.546	25.99	−1.388	< 0.43	< 0.80	P	7902	2.5	rp900171n00
171300.68+572530.2		0.360	18.85	−22.92	1.71	29.74	0.553	0.112	25.56	−1.606	1.25	2.63	P	5311	18.6	rp600425n00
171330.21+644253.0		1.048	18.11	−25.69	2.95	30.93	0.725	0.222	26.80	−1.583	< 1.50	< 3.00	R	3759		rs930521n00
171352.42+584201.2		0.521	18.77	−24.08	2.06	30.16	< 0.378	< 0.086	< 25.78	< −1.682	< 1.50	< 2.54	P	7902	15.7	rp900171n00
171359.52+640939.5		1.363	19.02	−25.61	1.46	30.84	0.286	0.101	26.68	−1.598	< 1.50	< 6.03	P	14534	11.6	rp800512n00
171441.87+644155.2	HS 1714+6445	0.285	18.88	−22.01	1.66	29.52	6.13	1.17	26.37	−1.210	< 1.50	< 4.27	R	3759		rs930521n00
171522.17+573626.6		2.030	17.53	−27.97	6.31	31.80	0.871	0.394	27.59	−1.614	< 0.44	< 0.51	P	5311	10.6	rp600425n00
171622.57+551213.4		0.323	19.04	−22.43	1.44	29.57	2.99	0.591	26.18	−1.300	< 0.45	< 1.16	R	1233		rs930729n00
171750.59+581514.0		0.310	17.76	−23.35	4.67	30.04	3.04	0.595	26.15	−1.495	< 0.41	< 0.41	R	1747		rs930729n00
171821.03+564551.3		0.619	22.35	−22.16	0.11	29.03	< 0.448	< 0.108	< 26.03	< −1.151	< 0.41	< 6.13	H	16225	6.3	rh801039n00
171845.14+562419.7		1.422	19.50	−25.25	0.91	30.67	< 0.228	< 0.083	< 26.63	< −1.552	< 0.42	< 2.62	H	16225	15.8	rh801039n00
171901.69+564657.8		3.920	20.19	−26.37	0.50	31.17	< 0.324	< 0.238	< 27.85	< −1.276	< 0.44	< 9.90	H	16225	9.8	rh801039n00
171901.70+580028.7		0.774	19.23	−24.00	1.18	30.27	< 0.364	< 0.096	< 26.18	< −1.569	< 0.44	< 2.02	P	5336	13.0	rp200724n00
171902.29+593715.8		0.179	18.23	−21.88	3.03	29.36	4.88	0.858	25.82	−1.362	< 1.50	< 1.71	R	2035		rs930624n00
171954.27+563103.2		3.211	19.36	−26.72	1.00	31.33	< 0.260	< 0.163	< 27.55	< −1.454	< 0.45	< 4.65	H	16225	16.2	rh801039n00
172026.69+554024.1		0.359	17.39	−24.05	6.57	30.33	3.39	0.687	26.34	−1.528	< 0.44	< 0.32	R	1287		rs930729n00
172032.28+551330.2		0.273	18.50	−22.41	2.36	29.63	2.94	0.558	26.01	−1.392	< 0.40	< 0.71	R	1312		rs930729n00
172059.46+612811.8		0.236	19.25	−21.68	1.18	29.20	2.05	0.377	25.71	−1.342	< 1.50	< 3.78	R	2016		rs930624n00
172100.76+632730.6		0.464	20.00	−22.36	0.65	29.55	0.937	0.205	26.05	−1.343	< 1.50	< 9.46	R	2417		rs930624n00
172122.82+575029.4		1.817	18.23	−26.79	2.79	31.35	< 0.240	< 0.100	< 26.91	< −1.706	< 0.41	< 1.09	P	5336	11.4	rp200724n00
172200.14+644357.3		1.767	17.91	−27.05	3.56	31.44	4.68	0.193	27.17	−1.637	< 1.50	< 2.94	R	3697		rs930521n00
172358.01+601140.0		2.239	19.15	−26.86	1.91	31.35	0.806	0.390	27.66	−1.416	< 1.50	< 6.06	R	2182		rs930624n00
172430.50+543952.4		1.076	19.55	−24.99	1.14	30.54	1.26	0.391	27.07	−1.330	< 0.46	< 1.86	R	1499		rs930729n00
172446.40+603619.6		0.372	18.97	−22.65	1.53	29.73	1.01	0.206	25.85	−1.486	< 1.50	< 4.33	R	2335		rs930624n00
172543.18+580604.8		0.292	18.78	−22.42	1.82	29.58	3.68	0.710	26.17	−1.309	< 0.44	< 0.91	R	1638		rs930729n00
172823.60+630933.7		0.439	19.18	−22.93	1.32	29.81	0.670	0.144	25.85	−1.521	< 1.50	< 4.91	R	2404		rs930625n00
172842.94+611057.1		0.590	18.73	−23.98	1.92	30.24	1.75	0.416	26.57	−1.407	< 1.50	< 3.72	R	2538		rs930625n00
173203.10+611751.9		0.358	19.31	−22.41	1.12	29.56	1.07	0.216	25.84	−1.426	< 1.50	< 4.98	R	2683		rs930625n00
173229.42+564811.3		0.303	18.77	−22.50	1.84	29.62	2.45	0.476	26.03	−1.377	< 0.44	< 0.92	R	1883		rs930729n00
173348.81+585651.0		0.491	18.12	−23.96	3.29	30.31	2.13	0.475	26.47	−1.474	< 1.50	< 2.48	R	2135		rs930729n00
173721.14+550321.6		0.333	19.26	−22.41	1.17	29.51	1.65	0.372	26.01	−1.343	< 0.44	< 1.21	R	1643		rs930729n00
174146.49+540146.1		0.416	19.64	−22.41	0.83	29.56	1.85	0.391	26.23	−1.276	< 0.46	< 2.14	R	1686		rs930729n00
233642.61+001653.3		2.606	19.14	−26.64	1.20	31.26	< 0.350	< 0.140	< 27.33	< −1.510	< 0.45	< 3.14	H	15215	14.0	rh800856n00
233718.07+002550.6		2.046	19.32	−26.09	1.20	31.08	< 0.405	< 0.184	< 27.27	< −1.464	< 0.45	< 3.03	H	15215	10.9	rh800856n00
233722.01+002238.8		1.380	19.68	−25.13	0.97	30.67	< 0.478	< 0.170	< 26.92	< −1.442	< 0.42	< 2.71	H	15215	7.6	rh800856n00
233736.43+000950.7		1.136	19.18	−24.89	1.16	30.59	< 0.329	< 0.105	< 26.55	< −1.552	< 0.41	< 2.06	H	15215	6.4	rh800856n00
233739.12+002656.2		1.700	18.86	−26.11	1.62	31.07	< 0.441	< 0.178	< 27.11	< −1.520	< 0.46	< 1.93	H	15215	10.7	rh800856n00
234819.58+005721.4		2.163	19.10	−26.19	1.10	31.08	0.143	0.068	26.87	−1.616	< 0.42	< 2.89	H	46315	0.0	rh701577a01
234840.05+010753.5		0.719	18.61	−24.27	2.13	30.46	1.35	0.347	26.67	−1.454	< 0.45	< 1.36	H	46315	11.6	rh701577a01
235221.19−005125.9		0.438	19.68	−22.32	0.98	29.59	0.747	0.160	25.89	−1.419	< 0.45	< 2.59	P	6867	18.5	rp701406n00

Note. — Luminosities are computed using H_0=70 km s^{-1} Mpc^{-1}, Ω_{M}=0.3, and Ω_{Λ}=0.7. The upper limits are at the 3σ level.

[a]Alternative name as reported in the SDSS EDR catalog.

[b]Rest-frame flux density in units of 10^{-27} erg cm^{-2} s^{-1} Hz^{-1} (at 2500 Å) and 10^{-30} erg cm^{-2} s^{-1} Hz^{-1} (at 2 keV).

[c]Rest-frame luminosity density (erg s^{-1} Hz^{-1}).

[d]Galactic absorption-corrected flux in the observed 0.5–2 keV band in units of 10^{-13} erg cm^{-2} s^{-1}.

[e]Observed-frame 1.4 GHz flux density either from FIRST or NVSS (mJy).

[f]Radio-loudness parameter, defined as $R = f_{5\,\mathrm{GHz}}/f_{4400\,Å}$ (rest frame; e.g., Kellermann et al. 1989). The rest-frame 5 GHz flux density is computed from the observed-frame 1.4 GHz flux density assuming a radio power-law slope of $\alpha = -0.8$, with $f_\nu \propto \nu^{\alpha}$.

[g]X-ray instrument used in the analysis: R=*ROSAT* All-Sky Survey; P=Pointed *ROSAT* PSPC; H=Pointed *ROSAT* HRI; C=*Chandra* ACIS-S; X=XMM-*Newton* EPIC.

[h]Exposure time (s).

[i]Off-axis angle (arcmin).

[†]BALQSO.